ChemCatChem

Review
doi.org/10.1002/cctc.202301214

Chemistry Europe
European Chemical Societies Publishing

www.chemcatchem.org

Recent Progress in the Application of Transition-Metal Containing MFI topologies for NH_3-SCR-DeNO$_x$ and NH_3 oxidation

Magdalena Jabłońska,*[a] Matthew E. Potter,[b] and Andrew M. Beale*[c, d]

Transition metal-containing MFI-based catalysts are widely investigated in the selective catalytic reduction of NO_x with ammonia (NH_3-SCR-DeNO$_x$), and the selective catalytic oxidation of ammonia (NH_3-SCO) into nitrogen and water vapor. While MFI-based catalysts are less intensively studied than smaller pore zeolites (i.e., chabazite, CHA) they are still used commercially for these processes and are of great interest for future study in particular to better understand structure-activity relationships. Hierarchically porous MFI catalysts (containing both micropores and mesopores) often show enhanced catalytic properties compared to conventional (microporous) materials in both NH_3-SCR-DeNO$_x$ and NH_3-SCO. Thus, a critical overview of the current understanding of the salient physicochemical properties that influence the performance of these catalysts is examined. Furthermore, strategies for the development of ZSM-5 based catalysts with enhanced catalytic lifetime, supported by the investigations of reaction mechanisms are reviewed and discussed.

1. Introduction

Zeolites that can be described with the general formula of $M_{(x/n)}[(AlO_2)_x(SiO_2)_y]\cdot wH_2O$ (where M is the alkali or alkaline earth cation of valance *n*, *w* is the number of water molecules, and *x* and *y* are the total numbers of tetrahedra per unit cell), are crystalline aluminosilicates with a regular micropore system, high specific surface area, hydrothermal stability, acidity and ion-exchange properties. Such characteristics make zeolites attractive in areas such as adsorption, separation and catalysis, etc.[1–3] Zeolites have been especially successful in catalysis for emission control, in particular the limiting of NO_x emissions from diesel engines, using a sacrificial reductant such as NH_3. This has been driven by regional legislation (i.e., EU, US, China) with the upcoming Euro VII emissions legislation in 2026, set to restrict NO_x emissions from all internal combustion engines to 60 mg for every kilometer travelled.[4] NH_3 emissions standards had previously been introduced on heavy-duty diesel vehicles in 2015 in the previous Euro VI legislation in 2015, limiting NH_3 concentration limits, worldwide, to 10 ppm.[5] However, global NH_3 emissions from the transportation sector are thought to be highly underestimated due to the difficulty in measuring them.[6,7]

NH_3-Selective Catalytic Reduction (abbreviated as NH_3-SCR-DeNO$_x$) is an attractive and effective route to remove up to 95% of NO_x (the major cause of photochemical smog, acid rain and ozone depletion, etc.) from industrial off-gases and diesel engine exhausts.[8] In a typical configuration, exhaust gases are first cleaned up *via* a diesel particulate filter (DPF) to remove soot particles. The remaining emissions then flow into a monolithic SCR unit, the walls of which are coated with catalyst, causing the NH_3-SCR-DeNO$_x$ reaction to take place.[9] The standard SCR reaction (Eq. 1) utilizes equimolar amounts of NO and NH_3 to reduce the NO_x to N_2. The presence of NO_2 can also enhance the low-temperature activity, due to the occurrence of the so-called fast SCR reaction, which involves the reaction of NH_3 particularly with an equimolar mixture of NO and NO_2 (Eq. 2). While NO_2 can itself be reduced to N_2 (Eq. 3), it has also been linked with the production of N_2O (Eqs. 4 to 6), which is highly undesirable as it is a powerful greenhouse gas.[10] Since NH_3 is considered particularly toxic in NH_3-SCR-DeNO$_x$ technology, it is typical to find an NH_3 slip unit after the SCR unit for the oxidation of residual ammonia into nitrogen and water vapor (NH_3-SCO, Eq. 5).[11–13]

$$4NH_3 + 4NO + O_2 \rightarrow 4N_2 + 6H_2O \quad (1)$$

$$2NH_3 + NO + NO_2 \rightarrow 2N_2 + 3H_2O \quad (2)$$

$$4NH_3 + 3NO_2 \rightarrow 7/2N_2 + 6H_2O \quad (3)$$

[a] Dr. Eng. M. Jabłońska
Institute of Chemical Technology, Universität Leipzig, Linnéstr. 3, 04103 Leipzig, Germany
E-mail: magdalena.jablonska@uni-leipzig.de

[b] Dr. M. E. Potter
Department of Chemistry, University of Bath, Claverton Down, Bath, BA2 7AY, UK

[c] Prof. Dr. A. M. Beale
Chemistry Department, University College of London, Gordon Street, London, WC1H 0AJ, UK
E-mail: andrew.beale@ucl.ac.uk

[d] Prof. Dr. A. M. Beale
UK Catalysis Hub, Research Complex at Harwell, Rutherford Appleton Laboratory, Didcot, OX110FA, UK

Supporting information for this article is available on the WWW under https://doi.org/10.1002/cctc.202301214

$$2NH_3 + 2NO_2 \rightarrow NH_4NO_3 + N_2 + H_2O \quad (4)$$

$$NH_4NO_3 \rightarrow N_2O + 2H_2O \quad (5)$$

$$2NH_3 + 2NO_2 \rightarrow N_2O + N_2 + 3H_2O \quad (6)$$

$$4NH_3 + 3O_2 \rightarrow 2N_2 + 6H_2O \quad (7)$$

Many reports on using zeolite and zeotype catalysts for NH_3-SCR-DeNO$_x$ focus on species with a chabazite (CHA) framework. Such species are considered 'small-pore' zeolites as the pore-windows within the framework are made of just 8 T-atoms (SiO_4 or AlO_4 tetrahedra) and are just 3.8 Å in diameter. However, CHA species form a 3D cage-like structure, meaning that whilst the pore-windows themselves are small, they lead into a larger cage which is roughly 7×10 Å. Indeed copper-containing CHA-type zeolite and zeotype catalysts (i.e., Cu-SSZ-13 and Cu-SAPO-34) exhibit remarkable NH_3-SCR-DeNO$_x$ activity and high hydrothermal stability (even in the presence of H_2O and/or SO_2 impurities) under practical conditions although Cu-SAPO-34 is much less stable than the Cu-SSZ-13. However, the comparatively recent work on small pore CHA zeolites was inspired by earlier examples of MFI-based NH_3-SCR-DeNO$_x$ catalysts reported by Held et al.[14] in 1990 on Cu-containing ZSM-5, and Iwamoto et al.[15] in 1986 of the unique activity of Cu-ZSM-5 in NO decomposition, which has been the subject of numerous studies. Further, early reports of Fe-containing ZSM-5 were also reported by Iwamoto and Yahiro[16] in 1994.

Unlike the cage-like chabazite structures, the MFI structure is a channel system, where orthogonal intersecting channels run through the system. The pore diameters in ZSM-5 are larger than CHA, constructed from 10T atoms, with dimensions of either 5.1×5.5 Å, or 5.3×5.6 Å, depending on the direction of the pore. ZSM-5 possesses the MFI topology and is the Al^{3+}-containing analogue of silicalite and was first synthesized in 1972. ZSM-5 can have transition metal ions incorporated into it that readily undergo changes in redox state and perform NH_3-SCR-DeNO$_x$ behaviour. Amongst the transition metal cations examined (Cu^{2+}, Fe^{3+}, Mo^{3+}, Cr^{3+}, etc.), Cu- and Fe-containing ZSM-5 have proven to be the most active, and N_2 selective, and therefore have been extensively studied. ZSM-5-based catalysts are one of the most frequently studied NH_3-SCR-DeNO$_x$ reference-catalysts because of their low cost, high activity and N_2 selectivity. For example, Cu-ZSM-5 (among Cu-TNU-9, Cu-FER, Cu–Y) displays extraordinary activity in NH_3-SCR-DeNO$_x$, achieving 100% conversion at 175 °C with almost 100% selectivity for the formation of N_2. Ammonia oxidation is frequently studied in order to explain the catalysts' behavior above 300–350 °C in the NH_3-SCR-DeNO$_x$. Reviews about the catalyst investigation (including hybrid catalysts) and reaction mechanisms in NH_3-SCO can be found in the references.[12,17–19] However, drawbacks such as the undesirable low-temperature catalytic activity depending on the applied materials, poor sulphur and/or alkali-resistance and hydrothermal durability of these catalysts are still a concern. As such significant efforts have been made in optimising the activity of promising transition-metal containing MFI materials. The influence of the

Magdalena Jabłońska received her PhD (2014) degree from the Faculty of Chemistry of Jagiellonian University in Kraków under the supervision of Prof. Lucjan Chmielarz; and Eng. (2013) from the Faculty of Energy and Fuel of the University of Science and Technology (AGH) under supervision of Prof. Teresa Grzybek. Aferwards, she joined the group of Prof. Regina Palkovits at RWTH Aachen University as postdoctoral fellow (2014–2017). Since 2017, she is a Junior Group Leader at Leipzig University, Germany. Her research focusses on environmental catalysis and energy conversion.

Matthew Potter received his MChem, and PhD, both at the University of Southampton. In 2015 he worked as a Postdoctoral researcher at the Georgia Institute of Technology, USA on Carbon Capture, before returning to Southampton in 2016 as a Research fellow, and then a Senior Research Fellow. He moved to the Research Complex at Harwell, working for UCL, in 2022 working on operando spectroscopy. Matthew is now a Prize Fellow in Sustainable Chemical Technologies at the University of Bath, where he works on carbon capture, carbon utilisation, and understanding these processes using synchrotron-based characterisation techniques.

Andrew (Andy) Beale was awarded a BSc from the University of Sussex followed by a PhD at the Royal Institution of Great Britain. He then worked as a Postdoctoral researcher, VENI Research Fellow and Assistant Professor in the Department of Inorganic Chemistry and Catalysis, Utrecht University in the Netherlands. He returned to the UK in 2013 as an EPSRC Early career fellow. He is currently Professor of Inorganic Chemistry at UCL and Group Leader at the Research Complex@Harwell and Chief Scientific Officer of Finden Ltd. Current research interests concern the study of functional materials with in situ and operando methods.

specific method of introducing transitions metals into the MFI system, modulating the porosity and the precise reaction mechanism, primarily of Cu and Fe based MFI systems has been widely studied to obtain more active and efficient catalytic systems.

2. Transition-metal-based ZSM-5 catalysts

Cu-containing or Fe-containing ZSM-5 showed significantly more NO conversion than other transition-metal-based catalysts (i.e., V, Co, Cr, Mn, Fe, Ni, Cu and Zn)[30–32,33]. Thus, much research has focused on looking at Cu- (for 'low' temperature studies below 400 °C), and/or Fe-containing ZSM-5 (for 'high' temperature studies above 400 °C).[21–23]

Table SI1 and SI2 summarize the catalyst preparation, reaction conditions, and NO_x conversion in NH_3-SCR-DeNO$_x$ (above 80% and related by-products in the range), and NH_3 conversion in the NH_3-SCO (100% conversion and related by-products in the range). Although the catalysts differ significantly on the Silicon to Aluminium Ratio (SAR); n(Si)/n(Al), the introduced metal species, calcination conditions or hydrothermal aging, while the reaction conditions varied regarding the feed gas composition, total flow, catalyst dosage or measurement systems, etc., a rough comparison is still feasible.

Generally, such species are prepared by aqueous ion-exchange with metal precursors and also *via* impregnation (e.g.,[24,25]). To undergo ion exchange, a zeolite should have an overall 'net negative charge' which occurs when Al^{3+} ions substitute framework Si^{4+} ions, often resulting in a SAR. This net negative charge is countered by 'charge-balancing cations', which in the case of solid-acid zeolite catalysts are simply protons (Brønsted acid sites). By introducing an excess of other ions to the framework, it is possible to swap or exchange the ions, so long as the neutrality of the system is preserved.

Copper ions are introduced to the ZSM-5 zeolite as Cu^{2+} in solution, typically in the form of $[Cu(H_2O)_6]^{2+}$, whilst some $[Cu_n(OH)_m]^{(2n-m)+}$ polynuclear hydroxo complexes (e.g., $Cu(OH)^+$) have also being observed.[26] On reaching the exchange site, the Cu species will be partly dehydrated, where a variety of species can form, including isolated Cu^{2+}, $[Cu–O–Cu]^{2+}$, and CuO (or $Cu(OH)_2$ with pH greater than 6).[27–30] The precise copper species formed varies depending on the identity of the charge-balance cations of zeolite, the copper precursor and the SAR etc.

While the SAR, determines the capacity to introduce metal ions at exchange sites,[31] it also influences the type of metal species that can form. Work by Torre-Abreu et al.[32] studied the influence of SAR, at a constant copper loading of 1.4 wt% on MFI catalysts. It was shown that for Al-rich species (low SAR) copper mainly existed as isolated Cu^{2+} ions. However, in Al-poor species (high SAR), CuO species appeared together with Cu^{2+} and Cu^+ ions. Changes in the zeolite preparation temperature (100–170 °C) can be used to modify the framework SAR, and thus, the nature of copper species in the Cu-containing ZSM-5.[33] Long and Yang[34] as well as Qi et al.[35] reported decreasing NO conversion with increasing SAR over Fe-ZSM-5 with similar ion-exchange levels, i.e., Fe-ZSM-5 (SAR = 10–11) reached > 80% NO conversion at 400–550 °C.

Besides the differences in the SAR, the degree of copper exchanged in a system can also influence the catalytic activity. Park et al. investigated the influence of n(Cu)/n(Al) ratio on Cu-ZSM-5 species (SAR = 14) for the reduction of NO by urea, which is known to be a near-equivalent reaction to NH_3-SCR-DeNO$_x$.[36] It was determined that ~125% ion-exchange was optimal for NO reduction. This was attributed to the system having a sufficiently high Cu exchange value to prevent Cu^{2+} species redistributing on the surface, whilst also limiting the amount of Cu to prevent CuO formation. In 1994, Komatsu et al.[37] showed an increase in the specific catalytic activity of Cu-ZSM-5 in NH_3-SCR-DeNO$_x$ with an increase in n(Cu)/n(Al) from 0.145 to 0.975, identifying $[Cu–O–Cu]^{2+}$ as the active sites. A similar $[Cu–O–Cu]^{2+}$ species stabilized by NH_3 and located in super cages of Cu-exchanged FAU was also considered by Kieger et al.[38] as the active sites in NH_3-SCR-DeNO$_x$.

Cu^+ sites are produced from Cu^{2+} exchanged cations by the process of self-reduction during dehydration, typically in an O_2 lean gas stream.[39,40] The Cu^+ species are compensated by a single Al^{3+} whereas it is often thought that two Al^{3+} ions in proximity are required to compensate a bare Cu^{2+}.[41] Therefore, depending on the catalysts' SAR and copper loading, different copper species may be present, while both isolated Cu^{2+} and $[Cu–O–Cu]^{2+}$ (as the product of dehydrating of $Cu[OH]^+$ at exchange positions[42]) are considered as active sites in NH_3-SCR-DeNO$_x$.[9] Otherwise, some researchers (e.g.,[43]) claim abundant $Cu[OH]^+$ species are responsible for the low-temperature activity during NH_3-SCR-DeNO$_x$. In contrast Fe species mainly exist as mononuclear sites with Fe loading < 0.3 wt.%, while oligomeric clusters and Fe oxide aggregates will gradually appear with the increased Fe loading.[44]

The nature of the charge balancing cations can also influence the catalytic sites and overall activity. Sultana et al.[45,46] reported that Cu-ZSM-5 prepared from a Na^+ form precursor showed higher activity for NH_3-SCR-DeNO$_x$ than those prepared from an H^+ form precursor, owing to the existence of a larger number of Cu^+ species and easily reducible Cu^{2+} species. In contrast, Fe-ZSM-5 prepared from a Na-ZSM-5 precursor showed lower NO conversion in NH_3-SCR-DeNO$_x$ compared with those prepared from H^+ or NH_4^+ forms.[47–49]

Many studies have examined the impact of using different preparation methods,[50–54] comparing Cu-ZSM-5 for example, prepared by conventional ion-exchange (IE), conventional impregnation (IM), ultrasound-enhanced impregnation (UIM), and conventional deposition-precipitation (DP) using NaOH and homogenous deposition-precipitation (HDP) using urea,[55] where the following trend in NO conversion was observed: Cu-ZSM-5 (HDP) > Cu-ZSM-5 (UIM) > Cu-ZSM-5 (IM) > Cu-ZSM-5 (IE) > Cu-ZSM-5 (DP). The catalytic activity correlated with the acid site strength and the presence of reducible isolated Cu^{2+} species present. Peng et al.[54] reported that Cu-ZSM-5 synthesized *via* a one-pot method with 4.5 wt% Cu species showed 80% NO conversion at 250 °C although only 12% NO conversion above 550 °C, which is significantly higher than conventionally prepared catalysts (within the scope of this

study). Zhong et al.[43] reported a novel one-pot method using the Cu-$(EDA)_2$ complex as a template to synthesis Cu-ZSM-5 for NH_3-SCR-DeNO$_x$ and which showed enhanced activity at low-temperatures, achieving NO conversions above 90% between 155–400 °C.

For Fe-containing catalysts, Long and Yang and Brandenberger et al.,[22,56] found that Fe-ZSM-5 prepared by ion-exchange and solid-state ion-exchange (SSIE) were more active than catalysts prepared by CVD (Chemical Vapour Deposition) due to the greater quantity of tetrahedral Fe^{3+} species. Kögel et al.[57] however, observed superior activity for Fe-ZSM-5 prepared by SSIE. Fe-ZSM-5 catalysts prepared *via* CVD of $FeCl_3$ and *via* the mechanochemical treatment of a $FeCl_3$/H-ZSM-5 presented different results in NH_3-SCR-DeNO$_x$ and SCR with hydrocarbons,[58] which was attributed to the different quantities of aggregated Fe species present in the two catalysts. Panahi et al.[20] showed that the most important parameter during NH_3-SCR-DeNO$_x$ is O_2 concentration; followed by $n(NH_3)/n(NO)$ ratio and finally gas hourly space velocity (GHSV) of the reaction. The NO conversion to N_2 of 63.1% and 94.9% was observed at 250 and 300 °C, respectively under the obtained optimum conditions ($c(O_2) = 5$ vol.%, $n(NH_3)/n(NO) = 1–1.25$, and GHSV = 8000 h^{-1}). The presence of H_2O increases the NO conversion but this effect is particularly pronounced at higher temperatures where NH_3 oxidation becomes important. Yu et al.[59] pointed out the influence of calcination temperature in the preparation of Fe-exchanged ZSM-5. The highest activity was reached for the sample calcined at 600 °C (between 500–700 °C), with NO$_x$ conversion above 80% between 450 and 650 °C.

While copper and iron species have their individual merits for this reaction, combining the species was reported to eliminate more NO$_x$ across a wider temperature range than individual Fe- or Cu-based zeolite catalysts. This lead to several pioneering works dedicated to Cu–Fe-containing ZSM-5-based catalysts.[60,61] The simultaneous presence of iron and copper species results in additional Lewis acid sites, and increased redox capacity compared to the monometallic analogues.[61] Thus, by controlling the concentration of metal ions in the catalyst, it is possible to extend the NO$_x$ conversion temperature window.[62,63] Zhang et al.[61] investigated a series of Fe_x-Cu_4-ZSM-5 catalysts with a fixed 4 wt% of copper and variable iron loading (2-8 wt%). The results indicated that the highest activities were seen with Fe_4-Cu_4-ZSM-5, and was attributed to the formation of Fe–Cu nanocomposites with high dispersion, leading to >90% NO conversion between 200–475 °C. In another study, an optimum of (1.98 wt%) Cu-(0.92 wt%) Fe-ZSM-5 was found with >80% NO conversion between 200–550 °C.[64,65] Panahi et al.[63] evaluated and optimized the Fe–Cu–ZSM-5 preparation parameters (Fe loading, calcination temperature, and impregnation temperature) to determine that the optimum synthetic conditions for maximum NO conversion of 78.8% (with the predicted value of 79.4%) were estimated at 4.2 wt% Fe loading (with 5 wt% Cu loading), calcination temperature of 577 °C and impregnation temperature of 43.5 °C. Also, Komatsu et al.[66] found Cu-exchanged ferrialuminosilicate to be a better performing catalyst than Cu-ZSM-5 for NH_3-SCR-DeNO$_x$.

The improvements of this dual cation approach extends beyond the study of powders, as combinations of Cu-containing and Fe-containing ZSM-5 catalysts in wash coat layers have also attempted to widen the NO$_x$ conversion temperature window. Such materials include sequential brick catalysts comprising Fe- and Cu-containing zeolite monoliths, mixed catalysts comprising a washcoat layer having equal mass fractions of Fe- and Cu-containing zeolites, dual layer catalysts comprising monolith coated with individual layers of Fe- and Cu-containing of different thickness and mass fractions.[67,68] Metkar et al.[67] reported the dual-layer catalyst where a range of thin Fe-containing zeolites (33% of the total washcoat loading) were layered on top of a thicker Cu-containing zeolite layer (67%, Figure 1a) resulted in very high NO$_x$ removal efficiencies over a wide temperature range for both the standard and fast NH_3-SCR-DeNO$_x$ (Eq. 1, 2). Their further studies concerns the experimental and kinetic modelling study over commercial Fe-ZSM-5 and Cu-CHA catalysts.[68]

Besides Cu- and/or Fe-containing ZSM-based zeolites, other combinations of transition metals were reported, such as Cu–Zr/ZSM-5 (with nearly 100% NO conversion between 167–452 °C[69]); Ce/Cu/Fe-ZSM-5 (with more than 80% NO conversion between 275–600 °C[70]); Mn/ZSM-5 (with almost 100% conversion of NO$_x$ in the range of 150–390 °C[71]); or CoMn/ZSM-5 (active below 150 °C[72,73]), etc. Some hybrid ZSM-5-based catalysts have been also proposed in the literature, including work by Salazar et al.[74–77] who utilized hybrid catalysts consisting of Fe-ZSM-5 and NO oxidation components (e.g., Mn_2O_3, Ce–Zr, Mn–Cr or Mn–Cu mixed oxides, etc.). They reported that the activity of the hybrid catalysts strongly depends on the spatial separation between the oxidation and NH_3-SCR components, i.e., mixed components after grinding and pressing, the simple mixing of components and in two-layer or four-layer beds[75] (Figure 1b–c). The enhanced activity was observed only when the components are thoroughly mixed and pressed. However, no correlation between the fast SCR activity of the NH_3-SCR components and the activity of the hybrid was observed.[77] It has been suggested that unstable surface-active intermediates such as HONO may be responsible for the activity enhancement of the hybrid systems.[75]

3. Effects of sulfur poisoning and hydrothermal stability

Hydrothermal stability, hydrocarbon (HC) and $H_2O/CO_2/SO_2$ tolerance are the main challenges facing the practical application of NH_3-SCR-DeNO$_x$ and NH_3-SCO transition-metal-based catalysts for dealing with diesel exhaust emissions. Indeed sulfate species (i.e., $(NH_4)_2SO_4$, $NH_4(HSO_4)$ or $(NH_4)_2SO_3$) formed during NH_3-SCR-DeNO$_x$ in the presence of SO_2 (below 100 ppm) lead to the blocking of zeolite channels and thus catalyst deactivation. These sulfates decompose above 450 °C (causing reversible catalyst deactivation). However, copper sulfate spe-

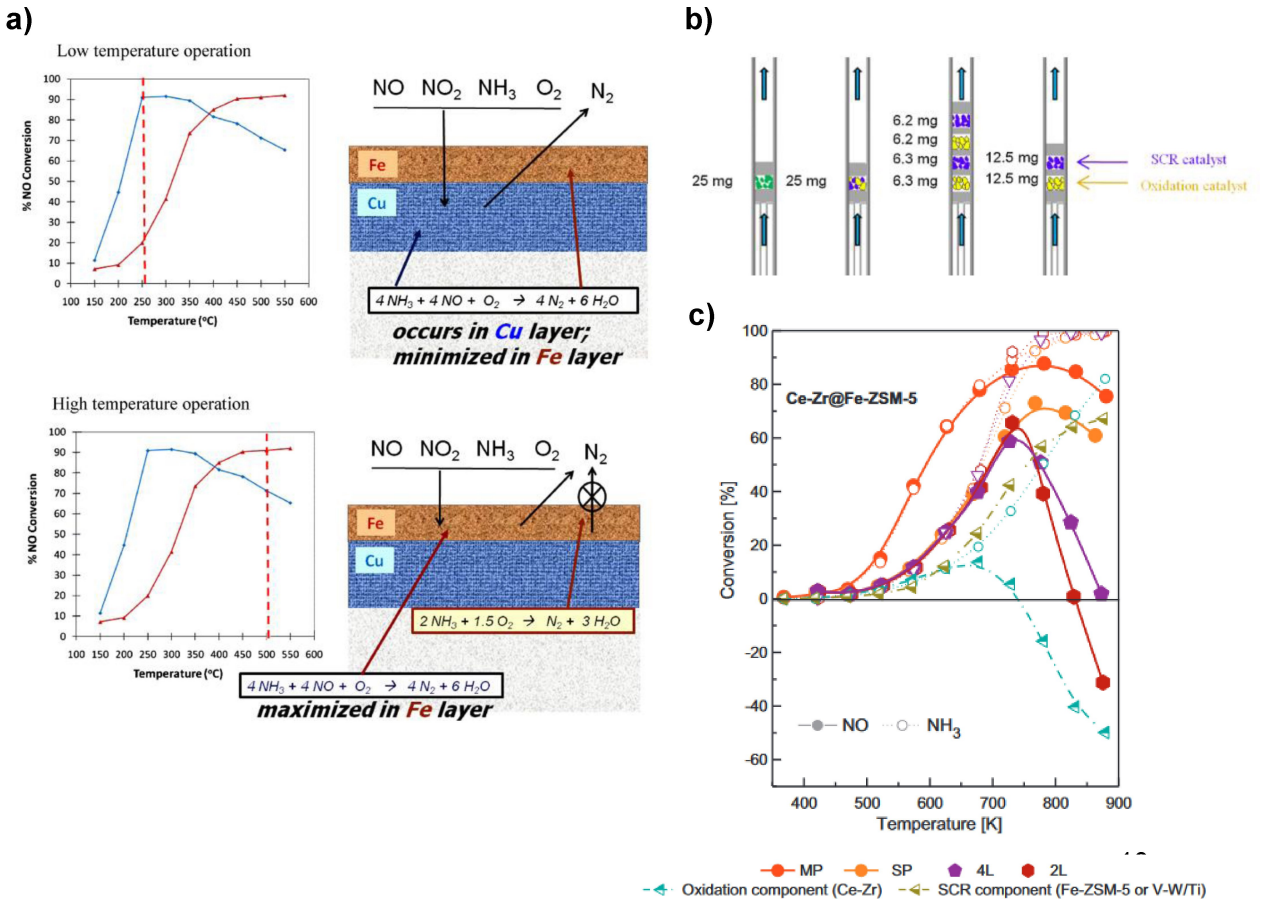

Figure 1. a) Schematic of the working principle of the dual-layer SCR catalyst at low and high temperatures. Reprinted from,[67] Copyright (2012), with permission from Elsevier; b) structure of catalyst beds: mixed particles (MP), separate particles (SP), four-layer arrangement (4 L) and two-layer arrangement (2 L), from left to right; and c) the influence of the particle separation on hybrid systems involving the Ce-ZrO_x oxidation component, Ce–Zr@VWTi. Reprinted from,[75] Copyright (2016), with permission from Elsevier.

cies can also form, which block the Cu^{2+} active sites and only decompose above 550–600 °C, leading to irreversible catalyst deactivation.[78] Cu-ZSM-5 catalysts typically suffer decreased (around 20 %) activity in the presence of 50 ppm SO_2 at 350 °C.[79] Modifying the species with silver, forming a Ag–Cu–ZSM-5 catalyst, showed that the species was unable to reach the same levels of NO conversion, after SO_2 had been introduced, and then removed from the feedstock, during time-on-stream studies at 300 °C,[80] demonstrating that while limited, some irreversible deactivation had occurred under these conditions. Fe– or Cu–Fe-containing catalysts are reported to be more sulfur resistant, both under dry and wet conditions than Cu-containing ZSM-5.[50,65,81,82] Silver et al.[83] reported that 350 ppm of S species did not significantly deactivate the Fe-containing zeolite SCR catalyst. Also, any further deactivation of Fe-ZSM-5 was only witnessed for the samples pre-treated at 700 °C for 24 h in air with 10 vol. % H_2O and 500 ppm SO_2, as opposed to those pre-treated only with water vapor.[35] Yuan et al.[53] drew similar conclusions, who observed minimal changes in the activity of Fe-ZSM-5 (prepared by one-pot hydrothermal synthesis) during NH_3-SCR-DeNO$_x$ in the presence of 50 ppm SO_2 and 3 vol.% H_2O at 350 °C.

Many studies have been performed looking at mitigating SO_2 poisoning below 350 °C, i.e., where the impact of sulfur poisoning is prominent. For example, modification of Cu-containing ZSM-5 with either Ce species[84] or ZrO_2[85] inhibits the deposition of $CuSO_4$ on the catalyst surface. For the optimized Cu–ZSM-5-ZrO_2 (2 wt %) catalyst, a high level of catalytic recovery of NO_x conversion was reported (below 300 °C), comparable with the non-poisoned catalyst.[85] Other catalysts including Co–Mn/ZSM-5,[72] Gd-MnO_x/ZSM-5,[86] Fe–W–Ni/ZSM-5[87] or W–Zr/ZSM-5[88,89] showed strong resistance against poisoning in SO_2 and H_2O. Here the NO conversion did not change in the presence of 5 vol. % of H_2O and 200 ppm of SO_2 in the feed over W–Zr/ZSM-5, though this study was carried out above 400 °C.[89]

Many researchers have tried to optimize the performance of MFI catalysts by the addition of other cations, such as Ce, Zr, and La or the introduction of extraframework Al in ZSM-5 zeolites etc. (e.g.,[85,90,91]). The temperature of the gas entering the NH_3-SCR device will periodically exceed 600 °C, due to the diesel particulate filter (DPF), being typically located before the SCR component. Despite this, few works report on catalysts tested above 500 °C (e.g., WO_3-ZrO_2 and ZSM-5[89]). Brandenberger et al.[48] reported that hydrothermal deactivation at

800 °C in 10 vol.% H_2O/air resulted in a greater decrease in the NH_3-SCR-DeNO$_x$ activity of Fe-exchanged Na-ZSM-5 than Fe-exchanged H-ZSM-5, though dealumination of the zeolite framework. Cu-ZSM-5 and Fe-ZSM-5 showed moderate hydrothermal stability when compared to small pore zeolites such as SSZ-13,[22,48,92] which was also reported to be due to dealumination and migration of Cu and Fe ions to form clusters or spinel phases.[93,94] Recently, Ye et al.[95] postulated that Cu^{2+} degraded into $[Cu_x(OH)_{2x-1}]^+$ oligomers/clusters, which can further grow into $Cu(OH)_2$ nanoparticles in steamed Cu-ZSM-5. This resulted in an unusual dip in NO conversion due to the undesired NH_3 oxidation over these species (Figure 2a); hydrothermal aging caused the decrease of NO oxidation activity and the Brønsted acidity of the catalysts.

We have previously discussed the role that the SAR and n(M)/n(Al) ratios have on determining catalytic activity, but many have shown that this also influences hydrothermal stability. Baik et al.[97] showed improved activity of Cu-ZSM-5 with n(Cu)/n(Al) = 0.585, but it possessed a lower hydrothermal stability compared to the sample with n(Cu)/n(Al) = 0.485. Zhang et al.[98] modified the surface of Cu-ZSM-5 by chemical liquid deposition (CLD) of tetraethoxysilane (TEOS), after aging at 750 °C for 13 h. The inert silica layer deposited on the surface formed a protective layer, which prevented the detachment of Cu^{2+} from ZSM-5 ion-exchange positions and the dealumination of zeolite during hydrothermal aging leading to N_2 selectivity above 90% over all fresh and aged catalysts. In another successful example, a core-shell structure zeolite with Fe-ZSM-5 core and ceria-loaded mesoporous-silica shell was prepared in order to accelerate low temperature NH_3-SCR-DeNO$_x$.[99] The enhanced activity (NO$_x$ conversion above 80% in the range of 270–480 °C with more than 98% N_2 selectivity) was ascribed to the occurrence of sequential reactions, in which part of the NO is oxidized to NO_2 in the Ce-loaded mesoporous silica shell, with NO_2 then mixing with the remaining NO leading to fast-SCR in the Fe-ZSM-5 core. The activity of core-shell samples was found to be much better that that of physically mixed catalysts. Similarly, Wang et al.[100] prepared a high-silica Cu-ZSM-5-PAD catalyst through effectively induced polymer (polyacrylamide) assisted deposition (PAD) strategy. The satisfactory hydrothermal stability (after treatment at 750 °C for 24 h NO$_x$ conversion exceeded 80% between 240–390 °C

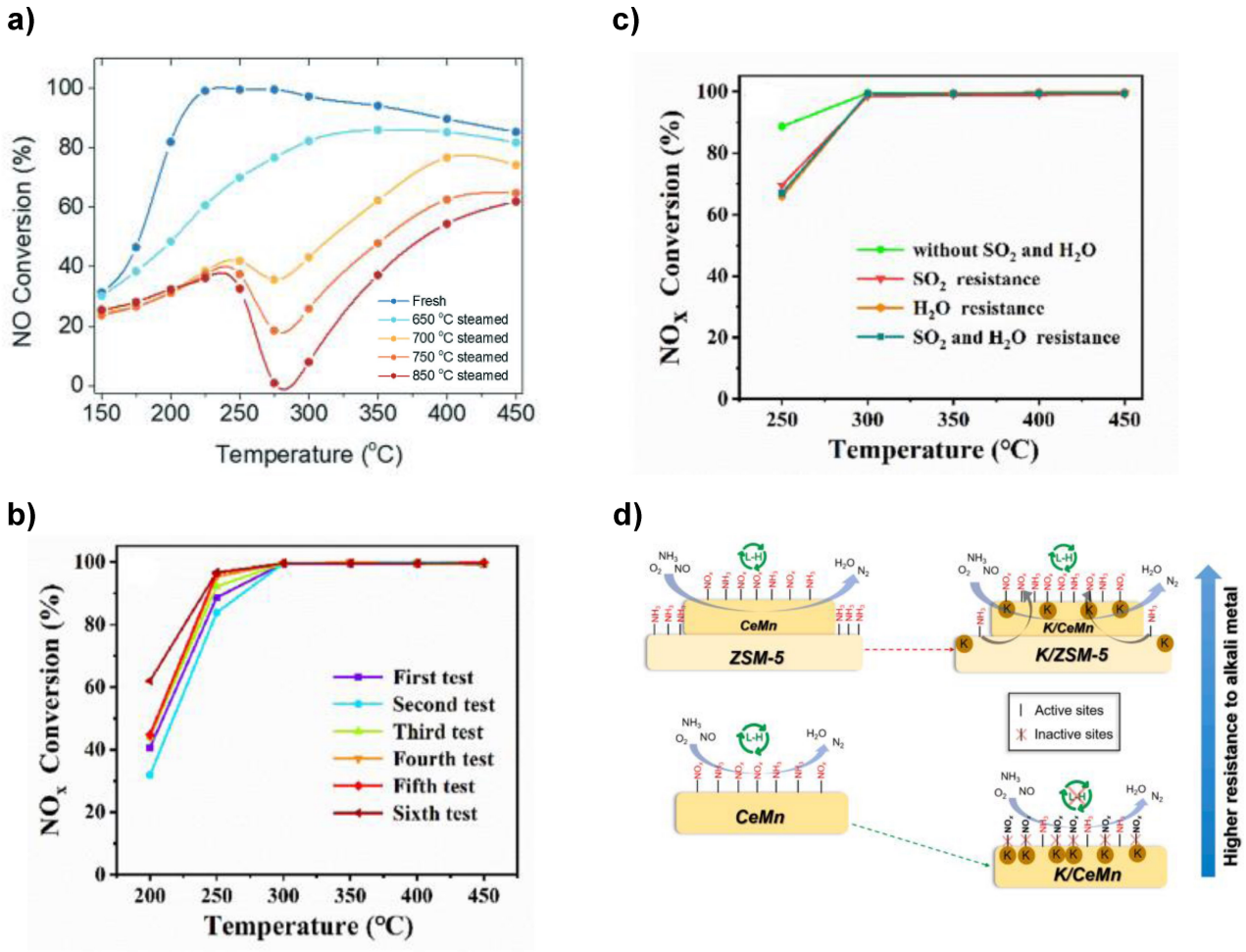

Figure 2. a) NO conversion during NH_3-SCR-DeNO$_x$ over fresh and steamed Cu-ZSM-5. Reprinted from,[95] Copyright (2022), with permission from The Royal Society of Chemistry; b) The results of NO$_x$ conversion during NH_3-SCR-DeNO$_x$ over CC–L2/Z5 Cu–Ce-La/ZSM-5 for recycling six times and c) the influence of SO_2 and H_2O on NO$_x$ conversion. Reprinted from,[90] Copyright (2022), with permission from Elsevier; d) schematic illustration of the anti-K poisoning mechanism over CeMn catalyst coupled with ZSM-5. Reprinted from,[96] Copyright (2022), with permission from Elsevier.

with more than 90% N_2 selectivity) and H_2O/SO_2 poisoning resistance are due to the encapsulation effect of the zeolite structure. Seo et al.[85] showed that the NO_x conversion of Cu-ZSM-5-(2 wt%) ZrO_2 was improved by 10–20% compared to that of reference Cu-ZSM-5 or Fe-containing zeolite catalyst (commercial) in the temperature range of 200–300 °C. Although the NO conversion of Cu-ZSM-5-(2 wt%) ZrO_2 decreased after hydrothermal aging (700 °C for 24 h), in the presence of C_3H_6 (due to the pore blocking), and sulfur poisoning, it's activity remained higher than Cu-ZSM-5-(0 or 4 wt%) ZrO_2. Yang et al.[90] doped various amounts (1-3 wt%) of La on Ce–Cu–ZSM-5 to improve stability, findings that 2 wt% of La was optimum. The redox cycle: $Cu^{2+} + Ce^{3+} \rightarrow Cu^{+} + Ce^{4+}$, facilitates electron transfer which promotes the oxidation of NO into NO_2 (fast SCR), while the presence of La increases the surface acidic and redox properties and is conducive to the creation of oxygen vacancies. Cu–Ce–La/ZSM-5 has shown outstanding stability during six consecutive experiments as well as excellent water and SO_2 resistance (Figure 2b–c). Furthermore, the addition of Ce or W improved the high temperature activity of Fe–Cu–ZSM-5.[101,102] WO_3/Fe–Cu–ZSM-5 catalysts have also been prepared using the SSIE method and aged at 850 °C for 5 h. The presence of tungsten oxide crystallites and iron oligonuclear clusters lead to improved activity at high temperatures, showing NO_x conversion below 70% between 450–550 °C, whereas the non-promoted Fe–Cu–ZSM-5 species achieved conversions below 60%.

Du et al.[103] constructed core-shell catalysts comprising 200 nm Fe-ZSM-5 particles coated with a silicalite-1 shell with an average diameter of 10 nm *via* secondary hydrothermal crystallization to improve the hydrophobicity of Fe-ZSM-5, and thus their activity and stability. Compared to Fe-ZSM-5 (NO_x conversion above 80% between 400–450 °C) with a similar Fe concentration, the core-shell zeolites achieve the same NH_3-SCR-DeNO$_x$ activity over a far greater temperature range (NO_x conversion above 80% in the range of 275–450 °C) and show greater resistance to hydrothermal aging. Chen et al.[91] deposited CeO_2 nanoparticles onto the surface of hierarchical Fe-ZSM-5 *via* dopamine polymerization. Fe-ZSM-5@CeO_2 exhibits a NO_x conversion over 90% and N_2 selectivity over 98% between 250–400 °C arising from improved oxidation of NO to NO_2 and further activation of the Fe^{2+}/Fe^{3+} redox-couple. The catalytic activity of Fe-ZSM-5@CeO_2 was unaffected by the presence of 10 vol.% H_2O. In contrast, the physically mixed Fe-ZSM-5 and CeO_2 showed poor NO_x conversion and N_2 selectivity, i.e., less than 20% NO conversion at 150–200 °C (with and without water vapor in the feed gas), emphasising the importance of using a hybrid system. A further motivation for working with hybrid catalysts includes expanding the functionality of such systems, e.g., to reduce SO_2 poisoning.[104] The CeO_2 shell of Cu/(ZSM-5@CeO_2) reacts with SO_2 preferentially leading to a higher sulfur tolerance due to limiting the formation of nitrate and ammonia sulfate species (blocking the pores and/or active sites), and copper sulfates. In summary, it has been shown that the application of hybrid catalysts is an effective approach enhancing both the activity and stability of NH_3-SCR-DeNO$_x$ catalysts.

The poisoning effect of alkali metals (e.g., Na and K) especially on zeolite-based catalysts and mainly for transition-metal-based catalysts has in contrast, seldom been reported. Jouini et al.[105] modified Cu–Fe–ZSM-5 with 1.5 wt% of Na and 1.8 wt% of K to simulate poisoning from exhaust gases of diesel engines and power plants. K resistance of Cu–Fe–ZSM-5 was better than Na resistance above 400 °C which was attributed to the stronger acidity and dispersion of metallic species of the resulting material, after K^+ addition. Ji et al.[96] reported a strategy to circumvent K poisoning of CeMn by physically coupling (*via* mechanical grinding) with ZSM-5. K_2O (0.5 wt%, 1 wt%, and 2 wt%) was deposited onto catalysts surface *via* impregnation. With ZSM-5 hybridization, the stable nitrates over CeMn can be facilely activated and consumed by NH_4^+ species introduced by ZSM-5, thus creating active sites and ensuring superior activity (Figure 2d).

4. Micro-/mesoporous ZSM-5-based catalysts

Intraparticle (pore) diffusion limitations are not restricted to a specific zeolite crystallite size in low temperature NH_3-SCR-DeNO$_x$.[106] For example, nanometer-sized Cu-ZSM-5 (~90 nm) showed a higher reduction rate of NO_x conversion than micrometer-sized Cu-ZSM-5. These observations indicate that diffusion of NO limits the apparent reaction rates, with some estimates suggesting only 36% of the active sites in zeolite crystals are utilized.[107] Cu-ZSM-5 catalysts with diverse morphologies (nanoparticles, nanosheets, hollow spheres) were compared with conventional Cu-ZSM-5.[108] It was found that Cu-ZSM-5 nanosheets, mainly dominated by the (010) crystal plane and whilst possessing abundant mesopores and framework Al species, led to the preferential formation of active copper species, and prompted rapid switching between Cu^{2+} and Cu^+ species during NH_3-SCR-DeNO$_x$, thus, exhibiting the highest NO conversion.

Pore diffusion can be improved by decreasing the diffusion length, this can be done a number of ways, including through the preparation of nanosized zeolites, or by modifying the pore structure of the catalyst by introducing meso- (2–50 nm) and/or macropores (>50 nm) into the zeolite crystals. Thus, the accessibility of the catalyst's active sites (located inside micropores) is improved. For purposes of the preparation of micro-/mesoporous, also called hierarchical (characterized by interconnected pore systems) zeolites or zeolites with inter-/intracrystalline mesopores in the literature, or even macroporous zeolites different approaches have been applied. Typically these methods can be divided into either a "bottom-up" approach, requiring the adjustment of the hydrothermal synthesis protocol, e.g., hard templating and soft templating, "top-down" methods, involving post-synthetic modifications of conventional zeolite crystals, e.g., demetallation, delamination and assembly procedures, or "mixed" techniques approaches have been applied, which are summarized in a number of publications.[109–121] Among these methods, the "top-down" method of exposing the synthesized zeolite to an alkali/acid solution treatment (breaking the Si–O–Al and Si–O–Si bonds) is

considered the most viable for large-scale industrial applications.[122–124] Typically, this is performed under fixed treatment conditions, i.e., optimized concentration, temperature and time of treatments, type of agent/presence of pore-directing agents (PDAs), stirring speed, etc. The benefits of a secondary pore system in zeolite catalysts have been reported in numerous studies, including in the field of environmental catalysis. Whilst there are many studies, which focus on the design and reaction mechanisms of microporous catalysts dedicated to NH_3-SCR-DeNO$_x$ or NH_3-SCO, studies on micro-/mesoporous catalysts are scarce. Chmielarz and Dziembaj reviewed layered zeolites (e.g., ITQ-2, MCM-36), their modifications and applications in NH_3-SCR-DeNO$_x$ and NH_3-SCO.[125] Thus, this review, for the first time summarizes bottom-up and top-down approaches for the preparation of the ZSM-5 zeolite-based catalysts investigated for NH_3-SCR-DeNO$_x$ and NH_3-SCO. The role of mesoporosity on performance is subsequently evaluated below.

The most common procedure for introducing mesoporosity into ZSM-5 crystals is desilication, typically using a 0.2 M NaOH or NaOH/TPAOH(TBAOH) solution for 0.5–5 h at 65–80 °C and ca. 3 g of zeolite per 100 ml of solution (e.g.,[118,126–130]). For example Góra-Marek et al.[130] prepared a set of ZSM-5 *via* a post-synthetic treatment (with NaOH and TBAOH) and a direct synthesis route with amphiphilic organosilanes, and introduced Fe *via* ion-exchange. These novel species showed an enhanced activity of micro-/mesoporous Fe-ZSM-5 (NO conversion above 80% in the range of 225–400 °C) compared to conventional sample (NO conversion more than 80% above 400 °C only). The enhanced mesopore volume of the zeolites was reported to prevent the clustering of introduced iron species and preserve them as isolated species inside the zeolite channels (Figure 3a). Additional research has also highlighted the benefits of mesoporosity for improved iron/copper dispersion[131–134] and metal loading. For example whilst parent microporous Cu-ZSM-5 achieved a maximum n(Cu)/n(Al) ratio of 0.18, after desilication for 6 h, a n(Cu)/n(Al) ratio of 0.48 was achieved. Similar work on Fe-ZSM-5 has also shown that desilication enhances the ion exchange properties.[131] Higher dispersion of iron species was also reported for mesoporous Fe-containing ZSM-5 (average diameter of 10–40 nm *versus* 10–80 nm for conventional ZSM-5) with the support synthesized by the introduction of a carbon matrix prior to its removal *via* calcination.[131] In contrast, Jabłońska et al.[126] found that the mesopores introduced by top-down treatment involving NaOH, TPAOH or a combination, into Cu-containing zeolite ZSM-5 catalysts do not play any direct role in the activity on NH_3-SCR-DeNO$_x$ (Figure 3b). Here, the post-synthesis modification of H-ZSM-5 with TPAOH allows for the introduction of a higher amount of Cu species (3.3 wt%, in aggregated form) compared to materials treated (before ion-exchange) with NaOH or NaOH/TPAOH, translating to a higher extent of ammonia oxidation above 350 °C. As mentioned before by Pérez-Ramírez et al.[135] the alkaline post-treatment led to mesopores with a broad distribution of around 10 nm, while the sharp peak at 4 nm appeared due to a 'tensile strength effect' (TSE).[136,137]

ZSM-5-based catalysts where the mesopores were introduced *via* direct synthesis were also widely investigated. Yue et al.[138] reported the depolymerization-reorganization method (from thermally activated diatomite and depolymerized rectorite) for the preparation of Fe-ZSM-5 with a uniform spheroidal morphology formed from densely stacked nanorods, leading to intercrystalline mesopores (ca. 10–50 nm, Figure 3c). Again, the highly dispersed Fe[138] led to enhanced NO_x conversion in NH_3-SCR-DeNO$_x$, (NO conversion above 80% in the range of 350–450 °C for mesoporous catalyst than below 50% for conventional sample under the same conditions) as did the copper-iron species.[139] Ma et al.[140] investigated mesoporous ZSM-5 prepared *via* a one-pot hydrothermal crystallization method in the presence of urea, as the support for Cu–Ce species. The high loading and enhanced dispersion of Cu and Ce species in mesoporous zeolite channels, compared to the conventional ZSM-5, were suggested as reasons for enhanced NO_x conversion (80% of NO conversion in the range of 200–450 °C). Cu-containing mesoporous ZSM-5 showed that as well as enhanced catalytic activity, the sulfur resistance is also improved, as the formation of sulfates on the catalyst surface is inhibited. For example, NO_x conversion below 350 °C, over micro-/mesoporous Cu-ZSM-5, was higher than for conventional catalysts when 100 ppm SO_2 was introduced to the feed gas.[141] In another approach, NO conversion of the CuFe-ZSM-5 catalyst decreases from 98 to 60% below 300 °C in the presence of 100 ppm SO_2 during NH_3-SCR-DeNO$_x$. Above 300 °C the conversion remains the same. In this case N_2 and N_2O selectivity were not affected by the presence of SO_2 in the feed.[139] The NO_x conversion decreased from 100% to 75% at 300 °C after the introduction of 5 vol.% H_2O and 100 ppm of SO_2 in the feed over mesoporous ZSM-5 zeolite embedded with MnCeO$_x$ catalyst.[142] The drop of NO_x conversion of 10% at 330 °C was reported for Fe-ZSM-5@Ce/mesoporous-silica in the presence of 10 vol.% H_2O and 500 ppm SO_2.[99] Significant sulfur resistance was reported also for other catalysts, including Fe-encapsulated ZSM-5 zeolite with nanosheet-assembled structure[143] and $Pr_xMn_{1-x}O_\delta$/3DOM ZSM-5.[144]

Although in some of the above studies the authors (e.g.,[130,140,141]) claimed that the presence of mesopores can enable faster transport of the reactants to active sites this proposal has not been confirmed experimentally. At least, the activation energy, the Thiele modulus and the effectiveness factor ($\eta = r_{obs}/r_{intrinsic}$, that relates the observed reaction rate and the intrinsic reaction rate) should be used as indicators of the presence or absence of diffusion limitations in mesoporous zeolites.[112,113,115] Metkar et al.[145] conducted an experimental study of mass transfer limitations in Fe- and Cu-zeolite-based NH_3-SCR-DeNO$_x$ monolithic catalysts with different lengths and loadings and concluded that in washcoated layers, diffusion limitation is present for NH_3-SCR-DeNO$_x$ between 250–450 °C for Cu-containing zeolite catalysts. Zhong et al.[146] developed a model describing NH_3-SCR-DeNO$_x$ and found that a small washcoat thickness (0.15 μm) and a large geometric surface area are advantageous leading to a reduction of the mass transfer limitation (Figure 3e). Yu and Zhang[147] developed a kinetic model and subsequent development of a novel Cu-ZSM-

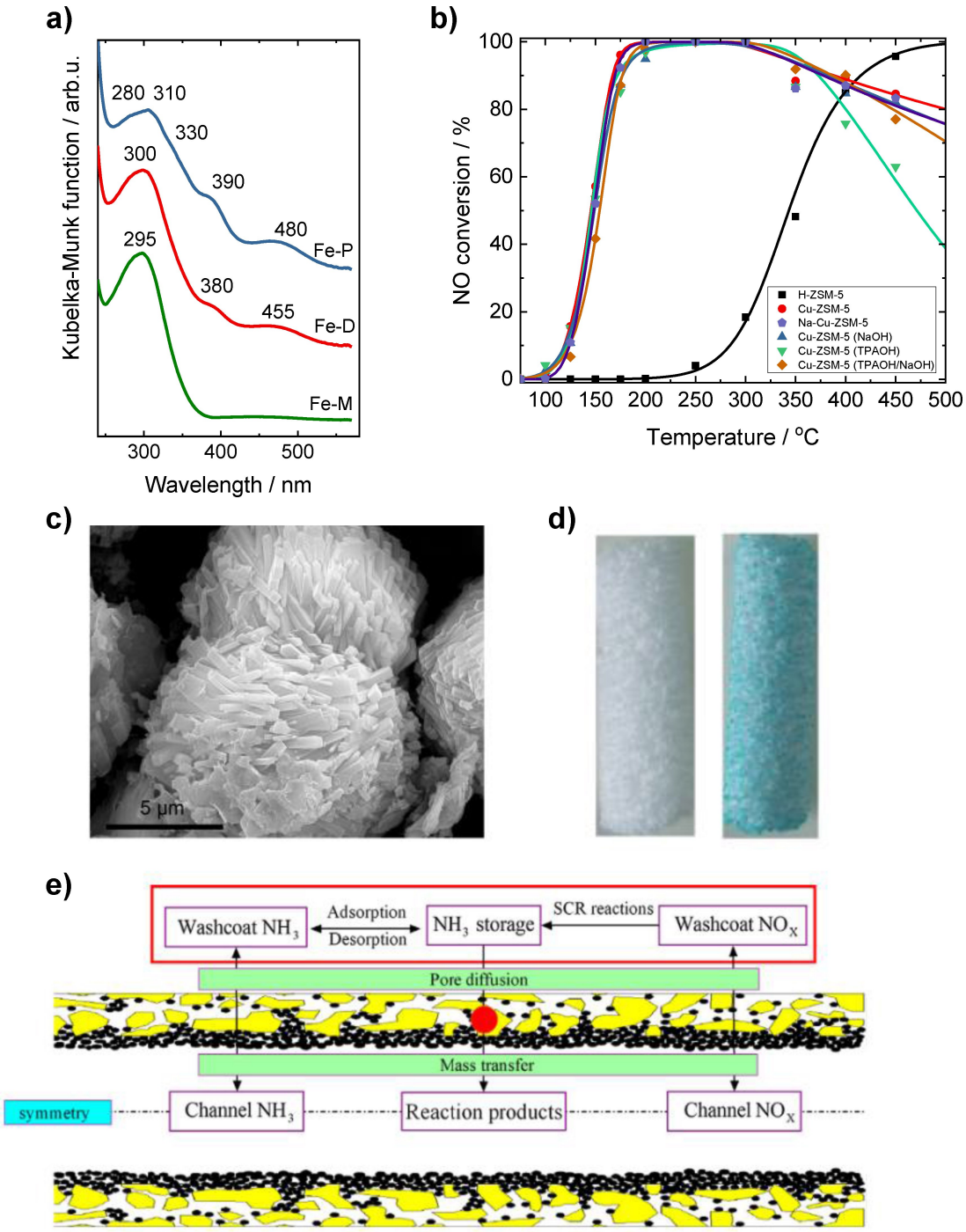

Figure 3. a) DR UV-Vis spectra of the Fe-containing ZSM-5; P (parent ZSM-5), D (desilicated ZSM-5), M (synthesized mesoporous ZSM-5). Reprinted from,[130] Copyright (2015), with permission from Elsevier; b) Experimental (points) and modelling (lines) results of NH_3-SCR-DeNO$_x$ over micro-/mesoporous Cu-containing ZSM-5. Reprinted from,[126] copyright (2021), with permission from MPDI; c) FESEM image of Fe-ZSM-5 synthesized *via* depolymerization-reorganization method. Reprinted from,[138] Copyright (2015), with permission from Springer Nature; d) Foam after *in situ* hydrothermal synthesis, and foam obtained after ion-exchange with copper acetate. Reprinted from,[149] Copyright (2022), with permission form the Royal Society of Chemistry; e) Schematic diagrams of a single channel of the flow-through model. Reprinted from,[146] Copyright (2019), with permission from Elsevier.

5 coated monolith channel for NH_3-SCR-DeNO$_x$. The hexagonal channel effectively increases the diffusion rate of reactants to the wall and the pressure drop resulting in improved catalytic activity. Recently, Jeong et al.[148] claimed that ceramic powder spray coating, resulted in super-strong adhesion of a Fe-ZSM-5 NH_3-SCR-DeNO$_x$ to stainless steel substrate without the use of binder.

Macroporous foam structures have also been coated with microporous or micro-/mesoporous zeolites to obtain porous systems,[117] such as Cu-ZSM-5 or USY (ultra-stabilized zeolite Y)

onto foams comprising α alumina,[149] FeCrAl[150–153] or SiC.[154] Geopolymers (GPs) which are considered amorphous analogues of zeolites, and known to be inherently macro-/mesoporous, possess high thermal stability and limited degradation of the structural network up to 800 °C have also been utilised. Cepollaro et al.[155] prepared geopolymer-based monoliths manufactured by direct ink writing, containing up to 60% by weight of pre-synthesized ZSM-5, and investigated their performance for NH_3-SCR-DeNO_x. Copper species were introduced as the active metal by ion exchange after preliminary acid treatment of the monoliths, leading to a structure with both macro-/mesoporous (geopolymer) and microporous (zeolite) phases. This approached allowed to achieve more than 80% NO conversion at 150–450 °C together with less than 25 ppm N_2O (Table SI2, pos. 14)

5. Reaction mechanisms

Langmuir-Hinshelwood (L–H; the reaction which occurs between adsorbed NH_3 species and adsorbed NO_x species), and Eley-Rideal (E–R; the reaction where adsorbed ammonia species is first oxidized to NH_x ($x < 3$) species by the high-valent redox sites, and then reacts with the gaseous NO_x species to generate N_2 and H_2O) mechanisms have both been proposed for NH_3-SCR-DeNO_x. These reaction mechanisms were primarily determined by analysing *in situ* DRIFTS spectra and related key intermediates that influence the activity of the catalysts. However, the reaction mechanisms over transition-metal ZSM-5-based catalysts are less extensively studied than Cu–CHA.[156,157] It has been proposed that the reaction mechanisms depend on the composition of the ZSM-5-based catalysts, the reaction temperatures, and pre-treatment conditions, all of which determine the active site, e.g., isolated Cu^{2+} in the fresh Cu-ZSM-5 and the $[Cu_x(OH)_{2x-1}]^+$ oligomers/clusters in the steamed Cu-ZSM-5 (e.g.,[23,95,158,159]). Grossale et al.[158] found that for the commercial Fe-ZSM-5 catalysts, NH_4NO_3 and NH_4NO_2 were formed *via* the L–H mechanism, from adsorbed NO_x species and the adsorbed NH_3 species, and then the nitrates decomposed rapidly to N_2 and H_2O. Feng et al.[89] confirmed the L–H mechanism (Eq. 8–17) over W–Zr/ZSM-5 using *in situ* DRIFTS, by identifying NH_4^+, surface-adsorbed NH_3 and amide ($-NH_2$) as the main reaction intermediates.

$$NH_3(g) \rightarrow NH_4^+ \quad (8)$$

(over zeolite Brønsted acid sites)

$$O_2 + 2^* \rightarrow 2\text{-}O^* \quad (9)$$

$$NH_3(g) + ^* \rightarrow -NH_3^* \quad (10)$$

$$-NH_3^* + -O^* \rightarrow -NH_2^* + -OH^* \quad (11)$$

$$NO(g) + -O^* \rightarrow NO_2^* \quad (12)$$

$$NO(g) + ^* \rightarrow -NO^* \quad (13)$$

$$-NH_2^* + -NO_2^* \rightarrow N_2 + H_2O + -O^* \quad (14)$$

$$-NH_3^* + -NO^* \rightarrow N_2 + H_2O + -H^* \quad (15)$$

$$NH_4^+ + \text{-}NO_2^* \rightarrow NH_4NO_2 \rightarrow 2H_2O + N_2 \quad (16)$$

$$2\text{-}NH_3^* + -NO_2^* + -NO^* \rightarrow 2N_2 + 3H_2O \quad (17)$$

Chen et al.[160] claimed that besides NH_4NO_2, adsorbed ammonia species and the nitrate and nitrite species also generate NH_2NO_2 and NH_4NO_3, where the latter could react with the adsorbed NO to generate N_2 and H_2O, and the NH_2NO_2 and NH_4NO_2 species could be decomposed to N_2 and H_2O at low temperatures over Mn–Ce/ZSM-5 (Eq., 18–23). However, at higher temperatures, the -NH_2 species would react with gaseous NO and NO_2 species to form NH_2NO and NH_2NO_2 intermediates, then decompose to N_2 and H_2O (Eq. 22 and 23) *via* the E–R mechanism:

$$NO_3^{-*} + NH_4^{+*} \rightarrow NH_4NO_3^* \quad (18)$$

$$2NH_4NO_3^* + NO^* \rightarrow NO_2^* + N_2(g) + 2H_2O(g) \quad (19)$$

$$NH_4^{+*} + NO_2^{-*} \rightarrow NH_4NO_2^* \rightarrow N_2(g) + H_2O(g) \quad (20)$$

$$\text{-}NH_2^* + NO_2^{-*} \rightarrow NH_2N_2^* \rightarrow N_2(g) + H_2O(g) \quad (21)$$

$$\text{-}NH_2^* + NO(g) \rightarrow NH_2NO^* \rightarrow N_2(g) + H_2O(g) \quad (22)$$

$$\text{-}NH_2^* + NO_2(g) \rightarrow NH_2NO_2^* \rightarrow N_2(g) + 2H_2O(g) \quad (23)$$

The NH_3-SCR-DeNO_x of Mn–Ce/ZSM-5, Mn–Ce/Beta and Mn–Ce/FAU catalysts mainly followed the L–H mechanism at lower temperatures and the E–R mechanism at higher temperatures.[160] However, both E–R and L–H mechanisms applied to Mn/ZSM-5 at 150 °C, while only the E–R mechanism was identified over Mn/ZSM-5 at 300 °C. As for Co/ZSM-5 and Cu-ZSM-5, both pathways were seen to exist simultaneously at 150 and 300 °C.[161] Bin et al.[69] discovered that NH_3-SCR-DeNO_x over Cu–Zr/ZSM-5 mainly followed the L–H mechanism at 170 °C. Xue et al.[73] reported that at 150 °C, both E–R and L–H mechanisms apply to the Cu-ZSM-5 catalyst, but the E–R mechanism is dominant in the SCR reaction over the Mn_1Co_2/ZSM-5 catalyst, where the Mn_1Co_2/Cu-ZSM-5 catalyst combines the mechanistic characteristics of Cu-ZSM-5 and Mn_1Co_2/ZSM-5. In terms of speciation, bridged nitrates have been observed to be the main nitrate species on the Cu-ZSM-5 catalyst whereas the bidentate nitrate has been proposed as the dominant species in Mn_1Co_2/ZSM-5. Both species are observed on Mn_1Co_2/Cu-ZSM-5. At 150 °C, the bridged nitrate can react with the adsorbed ammonia species easily, but the bidentate nitrate in contrast fails to do so (Figure 4a).

The role of redox states on the mechanism has been investigated albeit to a limited degree. For example, Wang et al.[108] suggested that the nitrosamine and nitrite species are the main intermediates during the NH_3-SCR-DeNO_x on nanosheets (NS) Cu-ZSM-5 involving an E–R mechanism (based on

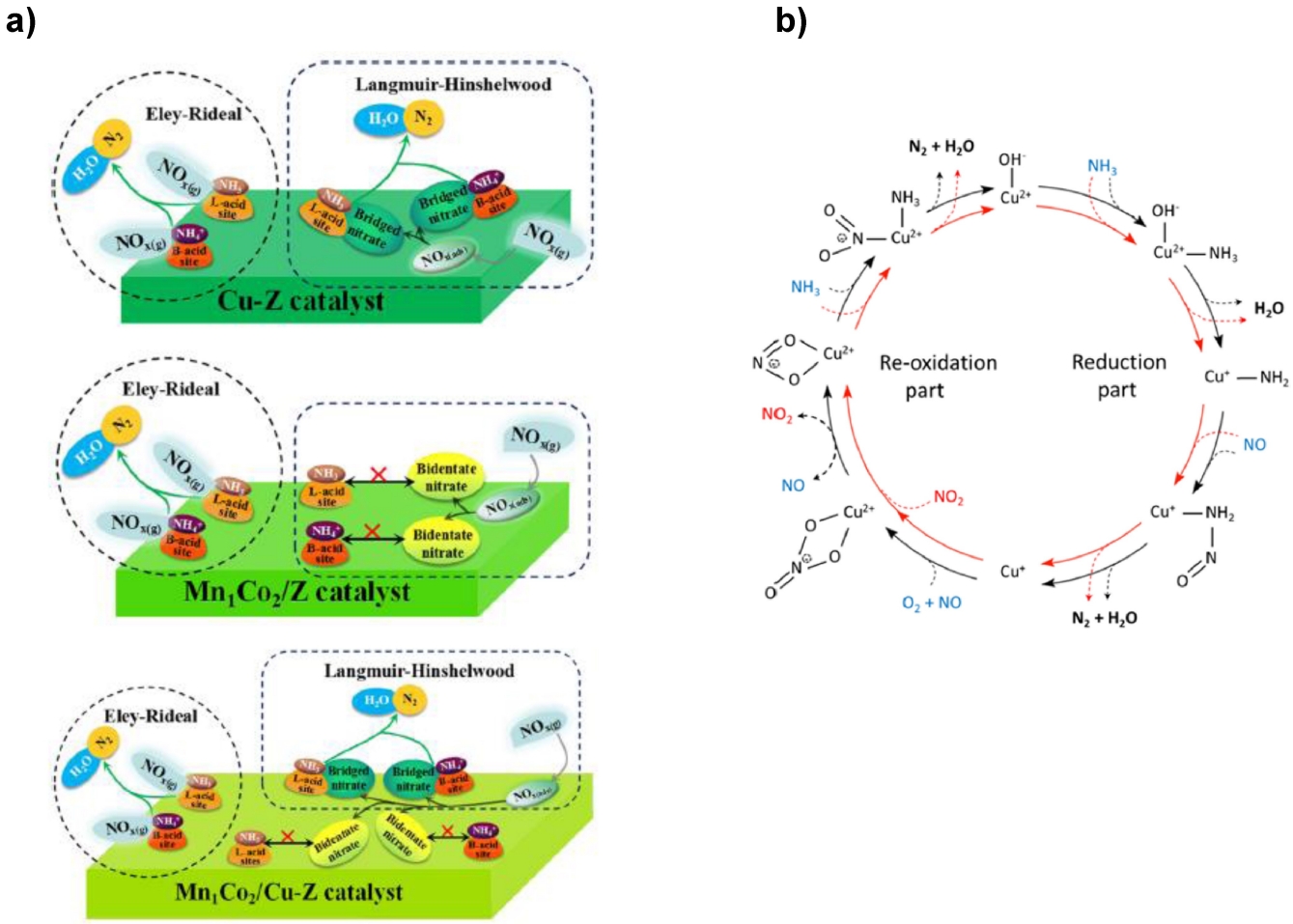

Figure 4. a) Proposed reaction mechanism of the NH_3-SCR-NO_x over Cu–Z, Mn_1Co_2/Z, and Mn_1Co_2/Cu–Z (Z – ZSM-5) catalysts at 150 °C. Reprinted from,[73] Copyright (2021), with permission from ACS Publications; b) proposed reaction mechanism of the NH_3-SCR-NO_x over NS–Cu-ZSM-5. Reprinted from,[108] Copyright (2021), with permission from ACS Publications.

in situ DRIFTS and DFT calculations). In the reduction part, the adsorbed NH_3 species on $[Cu(OH)]^+$ sites react with gaseous NO to form N_2 and H_2O. Here NO combines with NH_2 to generate nitrosamide species (NH_2NO) with Cu^{2+} reduction to Cu^+, and NH_2NO rapidly decomposed to N_2 and H_2O (Figure 4b). Recently, also Zhong et al.[43] claimed suggested that Cu-ZSM-5 (prepared *via* one-pot method, and thus possessing abundant $[Cu(OH)]^+$ species) mainly led to the formation of $[Cu(NH_3)]^+$-NH_2 and $[Cu(NH_3)]^+$-NO_2 intermediates. The $[Cu(NH_3)]^+$-NH_2 species, which originated from $[Cu(NH_3)_2(OH)]^+$ (L-NH_3), reacts with gaseous NO, forming N_2 and H_2O during the reduction-half cycle. In the oxidation half cycle, the $[Cu(NH_3)]^+$-NH_2 species transforms back to $[Cu(OH)]^+$ species (closing the catalytic cycle), in doing so, forming N_2 and H_2O. Yashnik and Ismagilov[162] observed that the total quantity of the TPD-desorbed NH_3, as well as the amount of ammonia coordinated in $[Cu(NH_3)_n]^{2+}$ complex, decreased with increasing sorption temperature, and under O_2–Ar or NO–O_2–Ar feeds for TPD mode. Cu^+ reoxidation to Cu^{2+} by NO and O_2, or NO_2, forms Cu–NO_2^-, which then reacts with NH_3 or NH_4^+ to yield N_2 and H_2O. However, for the other morphologies (i.e., nanoparticles, hollow spheres and conventional Cu-ZSM-5), the mechanism can vary.[108] Tarach et al.[163] reported that NH_3-SCR-DeNO$_x$ over the studied Cu-exchanged catalysts proceeds *via* $[Cu(OH)(NH_3)_3(NO)]^+$ intermediates (for the first time recognized by IR spectroscopy) followed by the reduction of Cu^{2+} to Cu^+ (based on rapid-scan FT-IR spectroscopy and two-dimensional correlation spectroscopy (2D COS)). Otherwise, Ruggeri et al.[164] conformed based on TPD experiments and *ex situ* FT-IR that the formed NO_2^-/HONO intermediates over Fe-ZSM-5 decompose into N_2 and H_2O during NH_3-SCR-DeNO$_x$.

6. In situ and operando studies for active site determination and mechanistic insight

There have been numerous *in situ* and *operando* spectroscopic studies looking at the active species and intermediates involved in the SCR process with the most popular methods being X-ray absorption spectroscopy and/or IR (typically DRIFTS). Many of these studies have been performed on Fe-ZSM-5 with analo-

gous studies performed typically on Cu-containing small pore zeolites (Cu-SSZ-13/Cu-SAPO-34). There is a general consensus on the nature of active species, with low nuclearity species typically being more active than polymeric or bulk species. Furthermore, most of the widely accepted mechanisms involve a redox cycle where nitrate and/or nitrite species, (that are regularly seen in IR studies) and have generally been proposed as being responsible for bringing about reoxidation of the active ions. Other species that have been observed and implicated in mechanistic studies include, metal-monohydroxy species, metal amines, and in computational studies and advanced spectroscopic measurements, intermediates such as nitrosamines have also been seen (*vide infra*). Although for Fe-based catalysts there is a clear benefit (higher NO_x conversion) to operating under fast SCR conditions, there are few studies that suggest the speciation and intermediates to be any different when compared to the standard SCR reaction. In the following section, we highlight some of the work which provided the basis for the above summary.

6.1. Fe-containing ZSM-5

One of the earliest studies that attempted to identify the active metal species involved in NH_3-SCR-DeNO$_x$ was from Kumar et al.[44] here, a series of Fe-ZSM-5 catalysts with different distributions of Fe sites were investigated using *in situ* diffuse reflectance (DR) UV-Vis, electron paramagnetic resonance (EPR), and FT-IR spectroscopy during interactions with the components involved in SCR of NO by NH_3 and i-butane. The catalysts ranged from those predominantly containing isolated Fe ions (Fe content $\leq$0.3 wt%) to those with additional oligonuclear Fe_xO_y clusters (0.6–0.7 wt% Fe) and large Fe_2O_3 particles. They showed *via in situ* FT-IR that the reduction of NO to N_2 in the presence of NO_2 and/or O_2 occurs through the formation of higher oxidized intermediates, such as adsorbed N_2O_4, N_2O_3, and nitrates, which are subsequently reduced. They concluded that the formation of nitrogen oxide intermediates in higher oxidation states requires the presence of trivalent active Fe sites, which undergoes a periodic Fe^{3+}/Fe^{2+} redox cycle. Fe sites that are permanently reduced to Fe^{2+} and cannot be reoxidized are likely inactive, as a Fe^{2+}/Fe^{+} redox cycle would be energetically unfavourable. These reduced Fe sites presented EPR signals at $g' \approx 6$ and partially at 4.3, while the EPR signal at 2 represented isolated reduction-resistant and potentially active Fe^{3+} sites. In contrast to isolated Fe^{3+} sites, oxidic clusters of varying sizes remained predominantly trivalent during the NH_3-SCR-DeNO$_x$, as indicated by DR UV-Vis signals above 300 nm and an EPR line at approximately $g' \approx 2$. These clusters exhibited slow reduction and rapid reoxidation, making them more oxidizing compared to isolated Fe^{3+} sites. This resulted in the undesired total oxidation of the reducing agent at higher temperatures.[165,166] Based on the findings of this study, a general rule for catalyst design was proposed, suggesting the concentration of accessible Fe^{3+} sites capable of participating in a reversible redox cycle should be maximized, while the formation of Fe_xO_y clusters should largely be avoided. In addition, the authors concluded that the zeolites Brønsted acidity was not a critical requirement for activity.

Similar conclusions were derived from work performed by Agote-Arán et al.[167] who used H-ZSM-5, Silicalite-1 and SSZ-13, with different Fe salts to produce catalysts with different Fe species. These were studied using a combination of high-energy-resolution fluorescence-detected XANES (HERFD-XANES) combined with valence-to-core X-ray emission spectroscopy (V2C XES) to obtain information about the oxidation state, coordination number, and ligand nature of the Fe sites in the presence of NO, NH_3 and during NH_3-SCR-DeNO$_x$. Whilst Fe/H-ZSM-5 contained isolated Fe^{3+} species with Oh and Td geometries, Fe/Silicalite-1 prepared with ferric citrate had dispersed Fe species in tetrahedral coordination, while Fe/Silicalite-1 prepared with ferric nitrate had increased amounts of Fe_xO_y clusters and Fe_2O_3 particles. Fe/H-SSZ-13 in contrast mainly consisted of large Fe_2O_3 particles. XES was used to identify that the dispersed Fe species in H-ZSM-5 showed a slight peak shift, indicating more ionic Fe–O bond character, compared to the Fe species in Silicalite-1. Changes in the HERFD-XANES during exposure to NO/NH_3 were observed only for Fe/H-ZSM-5, suggesting increased Fe coordination from NO adsorption, though under NH_3 flow or SCR conditions partial reduction to Fe^{2+} occurred. Fe/H-ZSM-5 exhibited higher NH_3-SCR-DeNO$_x$ activity, attributed to isolated Oh Fe^{3+} species with enhanced redox behavior, potentially facilitated by framework Al. In contrast, Fe/Silicalite-1 catalysts showed no spectral changes, suggesting the Td Fe^{3+} species had minimal interactions with reactants, while the activity observed was attributed to Fe clusters/particles. These observations suggest that the reducibility of Fe and its capacity to coordinate with reactant gases is important for low temperature activity.

A further study by Boubnov et al.[168] used the same X-ray methods to identify the reaction intermediates. Here Fe-ZSM-r was synthesized by a liquid ion-exchange with $FeCl_2$ to predominantly obtain monomeric Fe sites, as confirmed by DR UV-Vis spectroscopy and conventional EXAFS analysis. Pre-edge analysis using HERFD-XANES data, revealing the local chemical environment of Fe species in the as-prepared Fe-ZSM-5 catalyst can be described as an FeO_x moiety ($x=5$) and was consistent with Fe ions located in the cationic sites of the zeolite structure (i.e., α, β or γ sites).[165,166,169] Consistent with Agote-Arán et al.,[167] a dynamic chemical state between Fe^{3+} and Fe^{2+}, was observed, though this depended on the reaction conditions. Under oxidizing conditions, Fe predominantly existed as Fe^{3+}, while the addition of NH_3 slightly reduced the average Fe oxidation state. When NH_3 alone was fed, a significant fraction of Fe was reduced to Fe^{2+}. The coordination number of Fe in the catalyst varied between 4 and 5 under SCR conditions, and after the adsorption of pure NO. Analysis of the V2C XES emission lines revealed the presence of O, three-fold coordinated $O^{\delta+}$, and N atoms in the first coordination shell of Fe sites, which also indicated the formation of Fe–$O^{\delta+}$H–N intermediates. However, the coordination of NH_3 to Fe sites was hindered by the competitive coordination of water. Water vapor suppressed the direct coordination of NH_3 to Fe species and inhibited both NO oxidation and NH_3-SCR-DeNO$_x$ reactions.

Based on these findings, a mechanism for the NH_3-SCR-DeNO$_x$ was proposed involving the adsorption of NO on Fe^{3+} sites with partial reduction, followed by the adsorption of ammonia. High water partial pressure inhibited the reversible adsorption of NH_3, leading to the formation of nitrous acid and amine ligands. The reaction between these intermediates lead to N_2 and Fe^{2+} sites with lower coordination. A significant fraction of Fe^{2+} sites seen during SCR, suggested that the reoxidation of Fe^{2+} to Fe^{3+} was the slow, and potentially rate-limiting, step.

In a more recent twist to the study of active Fe species, Wierzbicki et al.[170] studied Fe-ZSM-5 catalyst prepared by introducing a Fe-EDTA complex into dealuminated ZSM-5, resulting in the formation of monomeric Fe species. This catalyst exhibited improved low temperature NH_3-SCR-DeNO$_x$ activity compared to a standard ion-exchanged catalyst. Both catalysts showed similar low selectivity toward N_2O and comparable high temperature catalytic activity. *In situ* XAFS data indicated the involvement of all Fe species in the redox activity of NH_3-SCR-DeNO$_x$. *Ab initio* simulations suggested that particularly active species adopted a square planar geometry when Fe ions were found in specific exchange positions (β sites) of ZSM-5, where the necessary number of Al pairs exist to force Fe into a square planar geometry. XAFS showed the square planar Fe species transitioned into five-fold coordination at low temperatures under reducing conditions, likely due to the adsorption of nitrogen oxide. Indeed, such results are consistent with previous assertions derived from EPR that mononuclear species sited in the β position of ZSM-5 are more readily reducible than those in the γ sites.

So, what are the cationic sites or locations inside ZSM-5? To date, the only detailed study on ion site location probably comes from Mentzen and Bergeret[171] with the results shown in Figure 5, which contains an illustration of the crystal structure of MFI with five cation locations for Cu^{2+} ions in ZSM-5 identified. Sites Cu1, Cu3, and Cu3′ in the ZSM-5 structure appear in the five- and six-membered ring subunits of the zeolite structure, which do not intersect with the main channels of ZSM-5. Sites Cu2 and Cu2′, which could account for ~ 60% of the total Cu content, were found in the vicinity of the ten-membered ring windows. Whilst this example specifically focused on Cu-ZSM-5, the findings apply equally to other M^{2+}-ZSM-5 species, including Fe-ZSM-5.

Typically, the most relevant and agreed-upon sites for metal cations in ZSM-5 are located in either the ten-membered ring channels or the channel intersections, coordinated to five- or six-membered rings (or in some cases, such as Cu2, to both), according to crystallographic locations. Employing the common notation used to differentiate the crystallographic sites, means cations Cu2 and Cu3 should be located in the as-labelled sites β and γ, respectively. Both are six-membered ring sites, however, with additional O–T–O bridges. The Cu2′ site, otherwise known as the δ site, is located in a five-membered ring structure.

In this vein, work by Vélez et al.[166] looked at differentiating the activity of such sites revealing that NO_2 and NH_3 adsorb at different sites, with NO_2 preferentially adsorbing at β-Fe sites and NH_3 adsorbing on Brønsted sites. Different nitrate species with varying adsorption strengths and reactivities are formed. In the presence of pre-adsorbed NH_4^+, a new type of nitrate species is identified, resulting from the interaction between NO_2 and neighboring NH_4^+. The formation of NH_4NO_2 and subsequent decomposition into N_2 and H_2O is suggested based on band shifts and the presence of nitrite species. *In situ* FTIR and EPR spectroscopic studies during standard and fast SCR reveal differences in adsorbed NH_3 concentration and iron nitrosyls. Fast SCR conditions lead to the accelerated formation of nitrates, followed by their reduction with NH_3 and NO. The reoxidation of Fe sites in both β and γ positions by NO_2 occurs at a lower temperature (150 °C) during fast SCR. Considering the spectroscopic findings, the role of NO_2 in fast reaction can be described as follows: NO_2 in the feed gas is rapidly converted to

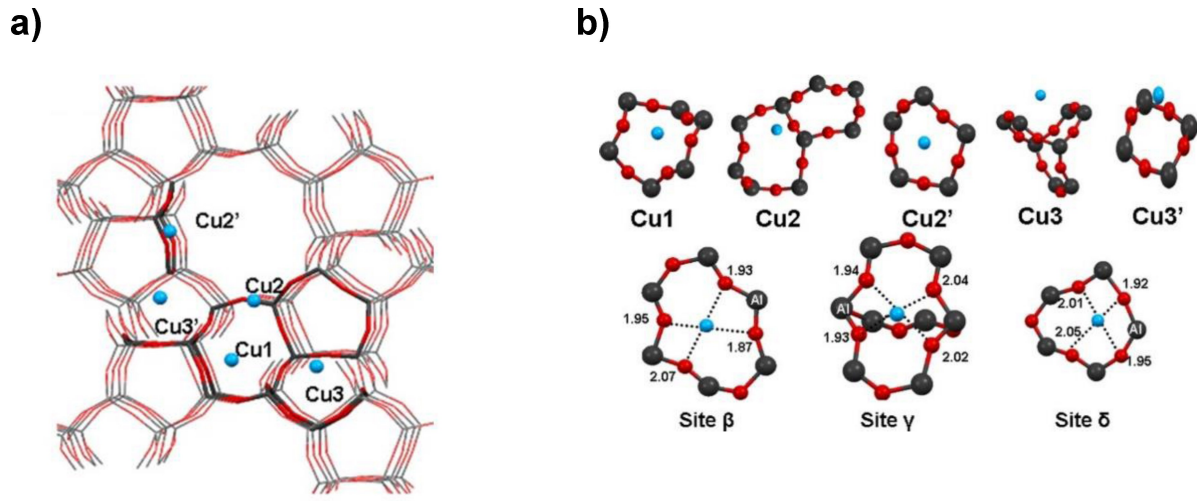

Figure 5. a) Crystallographic positions of Cu^{2+} (blue balls) in ZSM-5 (MFI framework) as proposed from single crystal XRD studies; b) Cu^{2+} local environment in zeolite ZSM-5. Top: Local environments of sites Cu1, Cu2, Cu2′, Cu3, and Cu3′ from the crystallographic model. Sites β, γ, and δ correspond to the local environments of Cu2, Cu3, and Cu2′, respectively. The final bond distances are as obtained from EPR and ab initio calculations. Reprinted from,[9] Copyright (2013), with permission from ACS Publications.

nitrates primarily adsorbed on β-Fe sites, facilitating the formation of NH_4NO_2. NH_4NO_2 subsequently decomposes into N_2 and H_2O. Fe sites in both β and γ positions remain in a redox-active state due to efficient reoxidation by NO_2, particularly under fast SCR conditions.

Finally regarding the properties of active Fe species, spatially resolved methods have been used to look at the spatiotemporal evolution of Fe redox and coordination state during NH_3-SCR-DeNO$_x$ and NH_3 oxidation.[172] A study by Doronkin et al.[172] investigated (0.5 wt%)Fe-BEA, (0.84 wt%)Fe-BEA, and (1.33 wt%)Fe-ZSM-5 catalysts, placed in a 1–1.5 mm quartz capillary (20 μm walls) which served as a plug-flow reactor. For time and spatially-resolved measurements, the catalyst bed (ca. 10 mm length) was divided into five evenly space zones with XAS spectra collected at all positions with an X-ray beam of about 200 μm ×200 μm. At high temperatures (T $>$250 °C) with varying NH_3 concentrations, the X-ray absorption edge shifted towards lower energies at the beginning of the catalyst bed, compared to the end, emphasizing the need for spatially-resolved analysis. The pre-edge feature of the XANES spectra also showed changes, with the centroid position shifting towards higher energies at the end of the bed, suggesting Fe oxidation with Fe reduction occurring at the start of the bed. Linear combination analysis using reference spectra revealed that NH_3 concentration affected the overall oxidation state, particularly at the inlet of the catalyst bed. The spatially-resolved study during NH_3 oxidation at 330 °C exhibited a similar gradient of oxidation state, indicating more reduced Fe sites in the first half of the catalyst bed. At higher temperatures, the zone with more reduced Fe sites shrank towards the bed's beginning due to increased reaction rates. Conversely, during NO oxidation or under air, no pronounced gradient of Fe oxidation state was observed. The gradients of Fe oxidation state were found not only for different Fe-containing zeolite catalyst compositions but also for different temperatures. The observed shifts in absorption edge and coordination sphere variations were attributed to the partial reduction of Fe sites by the reaction between adsorbed NH_3 and NO_x-derived species. The study also highlighted the NH_3 inhibition effect, primarily localized at the inlet of the catalyst bed, which could be attributed to NH_3 adsorption and blocking of Fe^{3+} sites, or stabilization of Fe^{2+} sites initially formed during SCR. Downstream in the bed, NO and NO_2 reacted following the standard or fast SCR mechanisms. At lower temperatures (T $<$250 °C), the spatially-resolved data showed an opposite trend, with the beginning of the bed being more oxidized than the end. The oxidation state of Fe species decreased as NO conversion increased and NH_3 concentration decreased along the bed. These findings provide insights into the chemistry of SCR and NH_3 oxidation reactions over Fe-containing zeolite catalysts, highlighting the role of spatial distribution and NH_3 inhibition effects.

In NH_3-SCR-DeNO$_x$, acidity is generally considered to be favorable, as acidic surfaces can adsorb NH_3 in large quantities, providing a reservoir of the reductant in the vicinity of the reduction site. In the mechanism suggested by Topsoe et al. for the V_2O_5/TiO_2 catalyst[173] an acidic V–OH group is also part of the active site, but some proposals do not involve the activation of NH_3 by a Brønsted acid site.[17] In an investigation of NH_3-SCR-DeNO$_x$ over VO^{2+}-exchanged ZSM-5, some of us concluded that the active site is a single VO^{2+} ion, which does not need the cooperation of Brønsted sites.[18] Li et al.[19] identified that the decomposition of an intermediate NH_4NO_2 is accelerated by zeolite Brønsted sites. Most studies have employed DRIFTS as the technique of choice for determining the reactivity of ammonium ions in the SCR reaction.

Schwidder et al.[174] performed one of the earliest studies examining the relationship between acidity and NH_3-SCR-DeNO$_x$ activity in Fe-MFI catalysts as a function of framework acidity and the Fe concentration (up to 1.2 wt% Fe). They observed that the low loading of Fe in Fe-silicalite led to the presence of primarily mononuclear Fe species whereas increasing Fe loading in Fe-ZSM-5 led to the formation of an increasing mixture of Fe species. NH_3-TPD profiles show a decrease in the high-temperature signal of zeolite Brønsted sites upon introduction of Fe species, accompanied by the appearance of a shoulder indicating NH_3 bound to Fe ions. Pyridine adsorption studies demonstrate the Lewis-acid character of Fe ions, with enhanced signals indicating increased acidity. The intensity of the Brønsted band remains similar in the sample with an intermediate concentration of Fe in H-ZSM-5, but this started to decline in samples with a higher Fe content. The catalytic data for NH_3-SCR-DeNO$_x$ suggested that there was no clear evidence for Brønsted acid involvement, with samples containing the most Fe (declining Brønsted acidity) showing the best activity and comparable performance for ZSM-5 samples with similar Fe loadings but different *n*(Si)/*n*(Al) ratio. Overall, catalysts with a combination of oligomeric Fe oxo clusters and Brønsted sites demonstrate higher activity in NH_3-SCR-DeNO$_x$; the authors proposed that a possible role of zeolite protons could be in performing acid-catalyzed decomposition of intermediate NH_4NO_2.

Ruggieri et al. studied the adsorption of NO_2 on Fe-ZSM-5 and the fast SCR reaction using a combination of *in situ* IR spectroscopy and flow reactor experiments, where it was found that the dominant and stable terminal products of NO_2 storage on the catalyst were ferric nitrates.[159] Other surface intermediates observed included NO^+ species resulting from the disproportionation or heterolytic chemisorption of NO_2, as well as Fe(II)–NO nitrosyls formed from NO adsorption on reduced Fe sites. Notably, the formation of nitrite intermediates was not detected, likely due to their high reactivity or their infrared features overlapping with those of the zeolite. However, despite their absence in the FTIR spectra, the role of nitrites in NO_2-related SCR chemistry was deemed to be highly probable (also suggested in the following work[175,176]). This is supported by additional FTIR runs demonstrating the significant reactivity of NO_2 with adsorbed ammonia, leading to the rapid conversion of NH_3 to nitrogen. Transient flow reactor experiments complemented these findings. They also concluded that the generation of nitrites and nitrates *via* NO_2 disproportionation likely contributed to the overall NH_3-SCR-DeNO$_x$ process. Further evidence supporting this pathway is the similarily observed between the surface ferric nitrates formed during the

steady state of the NH_3-NO_2 reaction and the surface condition obtained by exposing the clean catalyst to NO_2 without ammonia. They concluded that the reduction of surface nitrates by NO served as the rate-controlling step in low-temperature fast SCR chemistry. Furthermore, they hypothesised a cooperative interaction between acidic and redox sites in Fe-containing zeolite catalysts. The challenge when using any spectroscopic technique such as FT-IR, is differentiating between spectator and active species. To help in disambiguating the role of Brønsted acidity for the SCR reaction, a study by Chen et al.[177] utilised an innovative technique called *in situ* IS-DRIFTS (in situ impedance spectroscopy coupled with a DRIFTS spectroscopy) to investigate the proton transport properties and surface processes of Fe-ZSM-5 catalysts under SCR-related reaction conditions. Initially, DR UV-Vis and XPS confirmed the presence of isolated Fe species in Fe-ZSM-5 catalysts with low Fe loadings. *In situ* IS-DRIFTS measurements showed that with increased NH_3 loading, the proton conductivity of Fe-ZSM-5 catalysts increased, while the desorption or NH_3-SCR-DeNO$_x$ led to decreased conductivity. Furthermore, the authors were able to determine that the formation of NH_4^+ intermediates coincided with the increased activity of Fe-ZSM-5 in NH_3-SCR-DeNO$_x$, particularly at low temperatures. The study also revealed that the presence of isolated or dimeric Fe species in Fe-ZSM-5 with low Fe loadings contributed to higher reducibility and the formation of NH_4^+ intermediates, favoring the NH_3-SCR-DeNO$_x$ reaction.

6.2. Cu-containing ZSM-5

Cu-ZSM-5 is less studied than its Fe counterparts, perhaps because more interest has focused on studying small pore zeolites and zeotypes, particularly with CHA topology. However, an advantage of Cu over Fe is the extent of speciation with oligomers of Cu-oxy species (generally abbreviated to Cu_xO_y) being observed less frequently. As such there are more detailed mechanistic studies arising from the studies of Cu-based zeolites although there are many common reactant and intermediate species for both systems. A study by Kispersky et al.[178] compared the performance and behaviour of 2.7 wt% of Cu-ZSM-5, Cu-SSZ-13 and Cu-SAPO-34 using XAFS under *in situ* and operando conditions. The fitted XANES data indicated that the Cu-ZSM-5 catalyst consisted of a mixture of 65% Cu^+ and 35% Cu^{2+} during standard SCR, while under more oxidizing slow SCR, the catalyst was fully oxidized to Cu^{2+}. Furthermore, the authors compared the kinetics and rates of NO oxidation on the 2.7 wt% Cu-ZSM-5 catalyst measured in the *operando* reactor and a standard benchtop reactor, finding similar results. Rates of standard SCR on the three Cu-containing zeolite catalysts were also determined, with the ZSM-5 catalyst exhibiting the highest rates per mole of Cu. The amount of Cu^+ identified through XANES did not correlate with the SCR rate, indicating that both Cu^+ and Cu^{2+} species contribute to the catalytic activity. The specific zeolite structure influenced the relative fraction of Cu^+/Cu^{2+} under similar reaction conditions. The presence of Cu^+ and Cu^{2+} in the SCR redox pathway under standard SCR conditions was established, while in fast and slow SCR, Cu^+ was not detected, suggesting rapid re-oxidation of Cu^+ by NO_2. The presence of Cu^{2+} species during high NO_x conversion at temperatures in excess of 200 °C is regularly observed irrespective of zeolite topology, although at temperatures lower than this, Cu^+ species are often observed and implicated directly (as $[Cu(OH)]^+$) or indirectly as $Cu(NH_3)_2$ species that go on to form dimeric Cu oxo species.[179–181] We note however that the Cu oxo species thought to form in Cu-ZSM-5 and show activity in NO decomposition are not the same as those seen in SSZ-13 and which show low temperature NH_3-SCR-NO_x capability.[182]

Diffuse Reflectance (DR) UV-Vis under *in situ* conditions has also been used to understand Cu speciation on fresh and 850 °C steamed zeolite Cu-ZSM-5, showing the changes in LMCT (ligand-to-metal charge transfer) bands and their relation to ligand replacement (see Figure 6). The wavenumber at half height of the LMCT maximum was followed to examine ligand replacement during the NH_3-SCR-DeNO$_x$ reaction. The results indicated two regimes: a low temperature regime (150–250 °C) and a high temperature regime (300–450 °C). The LMCT band undergoes a gradual red shift with increasing reaction temperature, indicating the removal of NH_3 and stronger interaction with coordinated O_2^-. The d–d transition region in the DR UV-Vis spectra reveals different absorption bands corresponding to different Cu^{2+} geometries. The position and intensity of these bands change during the NH_3-SCR-DeNO$_x$ reaction, indicating the evolution of Cu^{2+} complexes. The contribution of tetragonally distorted and pseudo-tetrahedral distorted Cu^{2+} was prominent in both fresh and steamed Cu-ZSM-5. We note here that similar such species have also been seen in studies in Cu-SSZ-13, although differentiating between square planar and tetragonally distorted Cu^{2+} species often requires the use of computational methods, particularly to identify the nature of the axial ligand.[183,184] The results also suggest that the NH_3-SCR-DeNO$_x$ reaction proceeds through different mechanisms at different temperatures. At low temperatures (<250 °C), NH_3-SCR-DeNO$_x$ is the preferred reaction, and mobile $[Cu(NH_3)_4]^{2+}$ complex derived from isolated Cu^{2+} ions are proposed as the active site, although we observe the authors did not include such species in the rationalised reaction scheme in Figure 6. Cu aggregates were deemed responsible for the occurrence of unselective NH_3 oxidation, which affects the NO and NH_3 conversion in the reaction.

Operando DRIFTS spectroscopy data were also recorded in this study on fresh and steamed Cu-ZSM-5 catalysts, and after exposure to different gas flows. In the *operando* DRIFTS experiment on fresh Cu-ZSM-5, nitrates were formed in the presence of NH_3 and O_2, indicating the oxidation of surface NH_3. The formation of nitrates displaced pre-adsorbed NH_3 on Cu^{2+} sites. The Brønsted acid site reappeared, possibly due to the reaction between the Brønsted acid-adsorbed NH_3 (B-NH_3) and L-NO_3^-, followed by the restoration of the proton from NH_3 cleavage. The NH_3-SCR-DeNO$_x$ reaction occurred, involving NO and surface nitrates, leading to the formation of NO_2 and NO_2^-. Surface nitrites were not detected, but their presence was inferred based on nitrate depletion and the production of NO_2.

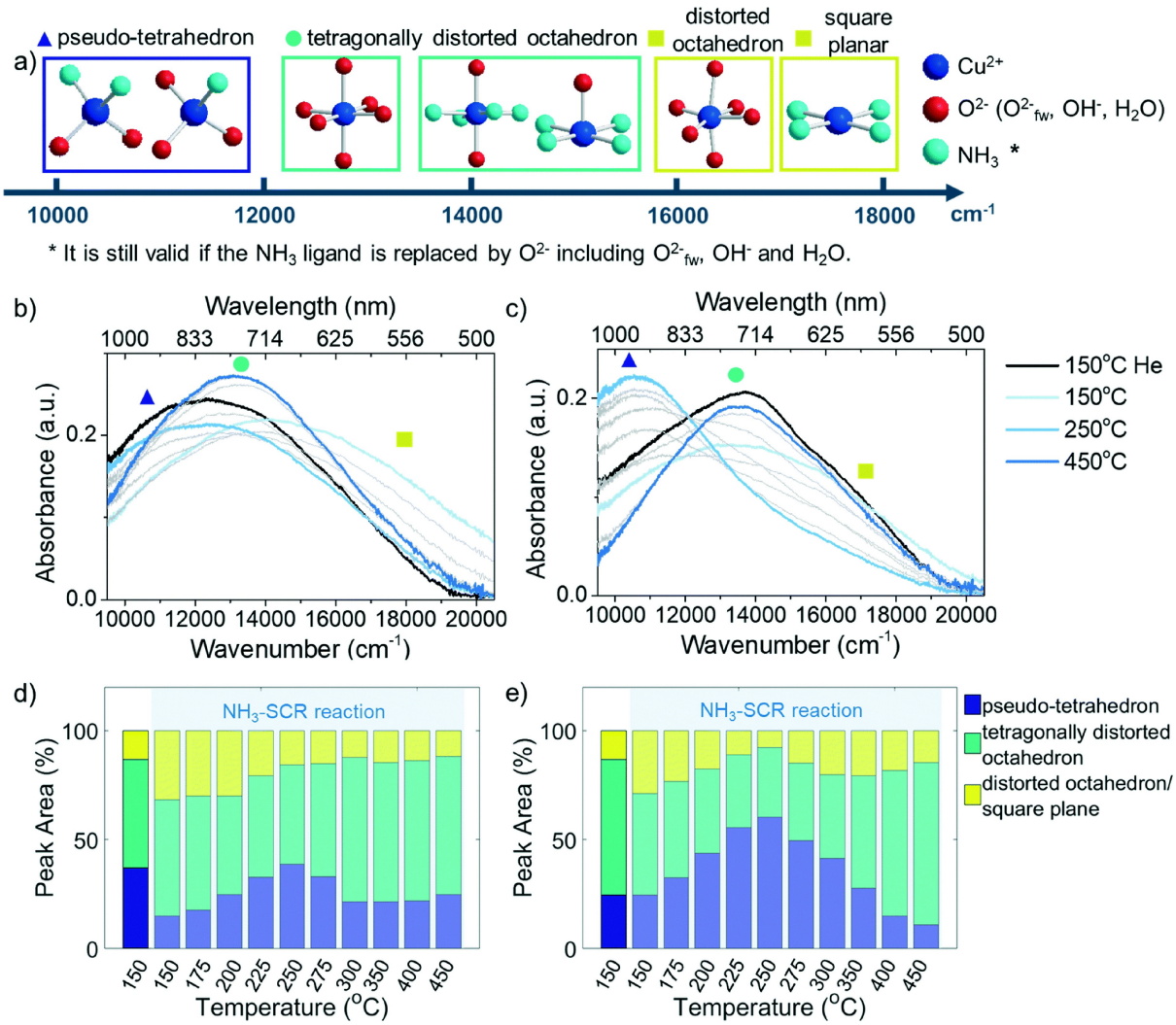

Figure 6. a) An illustration of the potential Cu-complexes found in Cu-ZSM-5 zeolite during the NH_3-SCR-DeNO$_x$ reaction with estimated wavenumber positions of their corresponding bands, determined by the ligand-field induced d-d splitting of Cu^{2+}. The NH_3-SCR-DeNO$_x$ reaction test measured the d-d transition band and peak fitting results of fresh (b and d) and 850 °C steamed (c and e) Cu-ZSM-5 zeolites, taken at steady-state conditions for each temperature. The grey-colored bands represent data collected at intermediate reaction temperatures ranging from 150–450 °C. In panel (a), the solid triangle (Prussian blue), circle (cyan), and square (yellow) indicate the positions of the main peak and shoulder in the spectra shown in (b) and (c). Reprinted from,[95] Copyright (2022), with permission from RSC Publications.

The steamed Cu-ZSM-5 catalyst exhibited different behavior in the *operando* DRIFTS experiment. Adsorbed NH_3 and nitrates initially formed, followed by the disappearance of both species and the increased adsorption of nitric acid. The competitive adsorption between NH_3 and nitric acid explained the NH_3 desorption. Nitric acid was reduced by NO, producing NO_2. The surface coverage of nitrates and nitric acid depended on the balance between their formation and consumption. The main reaction discussed in this study was the NH_3-SCR-DeNO$_x$ reaction, which involved the oxidation of NH_3 and the participation of surface nitrates. NO oxidation and NH_3 oxidation reactions contributed to the generation of NO_2. Nitric acid played a crucial role in the nitrate–nitrite equilibrium, which influenced the reaction selectivity. The participation of NO in the NH_3-SCR-DeNO$_x$ reaction occurred *via* the reaction with surface nitrates. The involvement of Brønsted acid sites in the NH_3-SCR-DeNO$_x$ reaction was not observed under steady-state conditions.

For completeness, we again revisit the question of Brønsted acidity for SCR in Cu-ZSM-5 using impedance spectroscopy. In a study, again by Chen and co-workers, the local dynamics of NH_3-solvated Cu species in Cu-exchanged zeolites under SCR-related model reaction conditions was investigated.[185] They focused on two types of zeolites: Cu-ZSM-5 (MFI) and Cu-SAPO-34 (CHA), using simultaneous *in situ* impedance and infrared 'modulus' spectroscopy, the researchers were able to directly probe the local dynamics of the Cu species as well as to monitor the ionic conductivity of the zeolite catalyst. The Cu-containing zeolites were first exposed to NH_3 until saturation and then to NO or NO/O_2 mixtures for surface reactions, and the DRIFTS spectra, as well as impedance signal (at a fixed frequency of 10 kHz for a higher time resolution), were collected simultaneously and continuously. They found that the

high-frequency ion movement, which corresponds to the short-range ion motion, was enabled by the co-adsorption and interaction of NO and NH_3 on Cu^{2+} sites since this led to the formation of highly mobile Cu^+ species and NH_4^+ intermediates, and, consequently, significantly enhanced local dynamics of Cu ions in both zeolite catalysts. This enhanced local movement of the exchanged Cu ions was attributed to NH_3-SCR-DeNO$_x$ conditions. It was observed that the solvation of zeolites with NH_3 led to two different ion movement processes: long-range transport across the zeolite lattice and short-range or local movement within a constrained space. Cu^+ species are more mobile than Cu^{2+} species, and under NH_3-SCR-DeNO$_x$ conditions, a fraction of Cu^{2+} can be reduced to Cu^+. The increase in the intensity of the NH_4^+ band corresponded to an increase in ionic conductivity, highlighting the significant impact of NH_4^+ intermediates on ion conduction within the catalyst. The re-oxidation of Cu^+, which is the rate-determining step of the NH_3-SCR-DeNO$_x$ reaction, was more favorable in Cu-SAPO-34 than in Cu-ZSM-5, which can be attributed to the close coupling of NH_4^+ intermediate and Cu site promoting the formation of Cu^{2+}-NO_2/NH_4^+. As a result, the overall local dynamics of Cu cations, largely determined by Cu^+ species, are less dependent on the NH_4^+ intermediate in Cu-SAPO-34 than in Cu-ZSM-5. The authors also concluded that the local motion of $Cu^{2+}(NH_3)(_n)$ species is favored within the CHA framework due to the unique cage structure and thereby contributes to the overall ion conductivity at high frequencies, which, on the contrary, is not observed for ZSM-5. Modulus spectroscopy or as it is more commonly referred as modulation excitation spectroscopy (MES) has been employed also to identify Cu-nitrosamines and Cu-nitrate species as intermediates in the NH_3-SCR-DeNO$_x$ reaction cycle.[186,187]

7. Conclusions

The NH_3-SCR-DeNO$_x$ is already a mature process as an enormous research effort has been dedicated to exploring the nature of the active sites and unravelling the reaction mechanisms. Still, due to a broad application of NH_3-SCR-DeNO$_x$ technology in stationary and mobile sources, it remains a popular subject for researchers working on improved/novel catalysts with enhanced activity, N_2 selectivity and lifetime. Especially, the investigation of the dynamic changes of the catalyst during hydrothermal aging, poisoning from multiple sources, as well as regeneration is still a challenging task.

While many different catalysts have been tested for this process, the overwhelming majority of studies focus on the use of either Cu, or Fe-based catalysts; this being due to copper having excellent low temperature SCR capabilities, whereas iron-based systems are more active at higher temperatures. Specifically in this review we have focussed on catalysts with the zeolitic ZSM-5 framework since there are several parameters which can be tuned, leading to different catalytic behaviour, most notably among these are the SAR, the initial charge balancing cations and the speciation and degree of ion exchange. Perhaps one of the most significant advantages of using ZSM-5 over the more recently intensively studied SSZ-13 topology is that the synthesis of the former is feasible using a wide range of organic structure directing agents and precludes the use of toxic HF. These many different variables can all significantly influence the catalytic activity, lifetime and the nature of the active site, meaning there is still significant scope for controlling the catalytic behaviour, even in systems with just a single metal, and a single species.

Given the copper and iron shown excellent activity, in different temperature zones, then a now popular method for extending the high-temperature window is combining monometallic MFI systems with a second component. We have presented examples of bimetallic Cu- and Fe- containing systems, and also shown the benefits of combining these monometallic species with secondary phases, such as CeO_2 to create hybrid catalysts with enhanced catalyst lifetime and improved resistance to poisoning from sulfur. This has seen researchers explore beyond simple powder mixing, to layered Fe and Cu washcoats on practical monoliths.

Another promising method to improve catalytic lifetime, being explored in many areas of zeolite catalysis is to incorporate other levels of porosity into the microporous framework, leading to the formation of mesoporous or hierarchical MFI zeolites. Whilst a range of synthetic techniques exist, by far the most applicable to large-scale industry are the 'top-down' desilication methods. Doing so not only modifies the systems porosity, to improve pore diffusion, but also allows different Cu and Fe-based active sites to form. The determined activation energies, Thiele modulus and effectiveness factor allow a more direct assessment of the presence of diffusion limitations in the mesoporous zeolites compared to conventional reference materials. As such SCR technology will continue to benefit from the growing toolbox of catalyst synthesis techniques, towards optimising catalyst behaviour. It is important however to not just vary synthetic parameters in a combinatorial manner, but also understand how catalysts degrade. As such there is still significant value in exploring the influence and interactions of poisons such as sulfates, alkali ions and even water vapour with metal-containing zeolites, as this unveils not just how to prevent deactivation, but also can provide vital insights into the nature of the active species.

Similarly, though many investigations have been carried out for reaction mechanisms still the NO reduction steps remain debatable due to difficulty in identifying reaction intermediates in NH_3-SCR-DeNO$_x$ over different catalysts and reaction conditions, etc. The difficulties appeared also, as the transition metal species located in zeolites have a very complex nature and they cannot be easily compared to the standard reference materials. Based on these combined spectroscopic, catalytic and DFT approaches should be utilized. Indeed, advances in *operando* spectroscopy, spatially-resolved techniques, and methods capable of distinguishing spectator and active sites, are providing greater insights into the NH_3-SCR-DeNO$_x$ systems under actual operating conditions, providing further insights into the mechanistic pathway.

Still questions remain about the precise reaction pathways, the influence of the zeolites Brønsted acidity, and the required

metal sites, providing new opportunities for the next generation of NH_3-SCR-DeNO$_x$ catalysts.

Acknowledgements

M.J. acknowledges a DFG Research Grant JA 2998/2-1. Open Access funding enabled and organized by Projekt DEAL.

Conflict of Interests

The authors declare no conflict of interest.

Keywords: ZSM-5 · NH_3-SCR-DeNO$_x$ · NH_3-SCO · reaction mechanisms

[1] Y. Li, L. Li, J. Yu, *Chem* **2017**, *3*, 928–949.
[2] Q. Zhang, J. Yu, A. Corma, *Adv. Mater.* **2020**, *32*, 2002927.
[3] Y. Li, J. Yu, *Nat. Rev. Mater.* **2021**, *6*, 1156–1174.
[4] Regulation (EC) No 715/2007. "Regulation (EC) No 715/2007 of the European Parliament and of the Council of 20 June 2007 on Type Approval of Motor Vehicles with Respect to Emissions from Light Passenger and Commercial Vehicles (Euro 5 and Euro 6) and on Access to Vehicle Repair and Maintenance Information.".
[5] EC-European Commission. "Commission Regulation (EU) No 582/2011 of 25 May 2011 implementing and amending Regulation (EC) No 595/2009 of the European Parliament and of the Council with respect to emissions from heavy duty vehicles (Euro VI) and amending Annexes I and III to Directive 2007/46/EC of the European Parliament and of the Council Text with EEA relevance.(Consolidated version)." *Off. J. Eur. Union* 167 (**2011**): 1–168.
[6] N. J. Farren, J. Davison, R. A. Rose, R. L. Wagner, D. C. Carslaw, *Environ. Sci. Technol.* **2020**, *54*, 15689–15697.
[7] W. Meng, Q. Zhong, X. Yun, X. Zhu, T. Huang, H. Shen, Y. Chen, H. Chen, F. Zhou, J. Liu, X. Wang, E. Y. Zeng, S. Tao, *Environ. Sci. Technol.* **2017**, *51*, 2821–2829.
[8] R. Chen, T. Zhang, Y. Guo, J. Wang, J. Wei, Q. Yu, *Chem. Eng. J.* **2021**, *420*, 127588.
[9] U. Deka, I. Lezcano-Gonzalez, B. M. Weckhuysen, A. M. Beale, *ACS Catal.* **2013**, *3*, 413–427.
[10] J. Han, A. Wang, G. Isapour, H. Härelind, M. Skoglundh, D. Creaser, L. Olsson, *Ind. Eng. Chem. Res.* **2021**, *60*, 17826–17839.
[11] T. Lan, Y. Zhao, J. Deng, J. Zhang, L. Shi, D. Zhang, *Catal. Sci. Technol.* **2020**, *10*, 5792–5810.
[12] M. Jabłońska, *Molecules* **2021**, *26*, 6461.
[13] M. Jabłońska, *ChemCatChem* **2020**, *12*, 4490–4500.
[14] W. Held, A. Konig, T. Richter, L. Puppe, *Techical Rep.* **1990**, *900496*.
[15] M. Iwamoto, H. Furukawa, Y. Mine, F. Uemura, S. Mikuriya, S. Kagawa, *J. Chem. Soc. Chem. Commun.* **1986**, *16*, 1272–1273.
[16] M. Iwamoto, H. Yahiro, *Catal. Today* **1994**, *22*, 5–18.
[17] M. Jabłońska, A. Mollá Robles, *Materials* **2022**, *15*, 4770.
[18] M. Jabłońska, R. Palkovits, *Appl. Catal. B* **2016**, *181*, 332–351.
[19] L. Chmielarz, M. Jabłońska, *RSC Adv.* **2015**, *5*, 43408–43431.
[20] P. N. Panahi, D. Salari, A. Niaei, S. M. Mousavi, *Chin. J. Chem. Eng.* **2015**, *23*, 1647–1654.
[21] P. Forzatti, I. Nova, E. Tronconi, *Angew. Chem.* **2009**, *121*, 8516–8518.
[22] S. Brandenberger, O. Kröcher, A. Tissler, R. Althoff, *Ind. Eng. Chem. Res.* **2011**, *50*, 4308–4319.
[23] P. Wang, D. Yu, L. Zhang, Y. Ren, M. Jin, L. Lei, *Appl. Catal. A* **2020**, *607*, 117806.
[24] P. N. R. Vennestrøm, T. V. W. Janssens, A. Kustov, M. Grill, A. Puig-Molina, L. F. Lundegaard, R. R. Tiruvalam, P. Concepción, A. Corma, *J. Catal.* **2014**, *309*, 477–490.
[25] B. Pereda-Ayo, U. De La Torre, M. J. Illán-Gómez, A. Bueno-López, J. R. González-Velasco, *Appl. Catal. B* **2014**, *147*, 420–428.
[26] S. A. Yashnik, Z. R. Ismagilov, *Kinet. Catal.* **2016**, *57*, 776–796.
[27] D. K. Lee, *Korean J. Chem. Eng.* **2004**, *21*, 611–620.
[28] T. Beutel, J. Sarkany, G.-D. Lei, J. Y. Yan, W. M. H. Sachtler, *J. Phys. Chem.* **1996**, *100*, 845–851.
[29] Y. Zhang, K. M. Leo, A. F. Sarofim, Z. Hu, M. Flytzani-Stephanopoulos, *Catal. Lett.* **1995**, *31*, 75–89.
[30] G. D. Lei, B. J. Adelman, J. Sarkany, W. M. H. Sachtler, *Appl. Catal. B* **1995**, *5*, 245–256.
[31] C. Torre-Abreu, M. F. Ribeiro, C. Henriques, F. R. Ribeiro, *Appl. Catal. B* **1997**, *11*, 383–401.
[32] C. Torre-Abreu, M. F. Ribeiro, C. Henriques, G. Delahay, *Appl. Catal. B* **1997**, *12*, 249–262.
[33] M. Jabłońska, K. Góra-Marek, P. C. Bruzzese, A. Palčić, K. Pyra, K. Tarach, M. Bertmer, D. Poppitz, A. Pöppl, R. Gläser, *ChemCatChem* **2022**, *14*, e202200627.
[34] R. Q. Long, R. T. Yang, *J. Catal.* **1999**, *188*, 332–339.
[35] G. Qi, Y. Wang, R. T. Yang, *Catal. Lett.* **2008**, *121*, 111–117.
[36] J.-H. Park, H. J. Park, J. H. Baik, I.-S. Nam, C.-H. Shin, J.-H. Lee, B. K. Cho, S. H. Oh, *J. Catal.* **2006**, *240*, 47–57.
[37] T. Komatsu, M. Nunokawa, I. S. Moon, T. Takahara, S. Namba, T. Yashima, *J. Catal.* **1994**, *148*, 427–437.
[38] S. Kieger, G. Delahay, B. Coq, B. Neveu, *J. Catal.* **1999**, *183*, 267–280.
[39] E. Broclawik, J. Datka, B. Gil, P. Kozyra, *Catal. Today* **2002**, *75*, 353–357.
[40] E. Broclawik, J. Datka, B. Gil, P. Kozyra, *Int. J. Mol. Sci.* **2002**, *3*, 435–444.
[41] J. Dědeček, B. Wichterlová, *P Phys. Chem. Chem. Phys.* **1999**, *1*, 629–637.
[42] V. L. Sushkevich, A. V. Smirnov, J. A. van Bokhoven, *J. Phys. Chem. C* **2019**, *123*, 9926–9934.
[43] C. Zhong, Y. Ren, C. Yin, R. Wang, J. Hou, L. Wang, Z. Zhao, B. Mozgawa, P. Pietrzyk, Z. Sojka, Y. Song, *ACS Catal.* **2023**, *13*, 10927–10944.
[44] M. S. Kumar, M. Schwidder, W. Grünert, U. Bentrup, A. Brückner, *J. Catal.* **2006**, *239*, 173–186.
[45] A. Sultana, T. Nanba, M. Haneda, H. Hamada, *Catal. Commun.* **2009**, *10*, 1859–1863.
[46] A. Sultana, T. Nanba, M. Haneda, M. Sasaki, H. Hamada, *Appl. Catal. B* **2010**, *101*, 61–67.
[47] J. A. Sullivan, O. Keane, *Appl. Catal. B* **2005**, *61*, 244–252.
[48] S. Brandenberger, O. Kröcher, M. Casapu, A. Tissler, R. Althoff, *Appl. Catal. B* **2011**, *101*, 649–659.
[49] X. Shi, H. He, L. Xie, *Chin. J. Catal.* **2015**, *36*, 649–656.
[50] A.-Z. Ma, W. Grünert, *Chem. Commun.* **1999**, *1*, 71–72.
[51] H.-Y. Chen, W. M. H. Sachtler, *Catal. Today* **1998**, *42*, 73–83.
[52] R. Q. Long, R. T. Yang, *J. Am. Chem. Soc.* **1999**, *121*.
[53] E. Yuan, G. Wu, W. Dai, N. Guan, L. Li, *Catal. Sci. Technol.* **2017**, *7*, 3036–3044.
[54] C. Peng, J. Liang, H. Peng, R. Yan, W. Liu, Z. Wang, P. Wu, X. Wang, *Ind. Eng. Chem. Res.* **2018**, *57*, 14967–14976.
[55] P. Nakhostin Panahi, D. Salari, H.-H. Tseng, A. Niaei, S. M. Mousavi, *Environ. Technol.* **2017**, *38*, 1852–1861.
[56] R. Q. Long, R. T. Yang, *Catal. Lett.* **2001**, *74*, 201–205.
[57] M. Kögel, R. Mönnig, W. Schwieger, A. Tissler, T. Turek, *J. Catal.* **1999**, *182*, 470–478.
[58] M. Schwidder, F. Heinrich, M. S. Kumar, A. Bruckner, W. Grünert, in *Studies in Surface Science and Catalysis*, Elsevier, **2004**, pp. 2484–2492.
[59] D. Yu, P. Wang, X. Li, H. Zhao, X. Lv, *Fuel* **2023**, *336*, 126759.
[60] H. Jouini, I. Mejri, C. Petitto, J. Martinez-Ortigosa, A. Vidal-Moya, M. Mhamdi, T. Blasco, G. Delahay, *Microporous Mesoporous Mater.* **2018**, *260*, 217–226.
[61] T. Zhang, J. Liu, D. Wang, Z. Zhao, Y. Wei, K. Cheng, G. Jiang, A. Duan, *Appl. Catal. B* **2014**, *148–149*, 520–531.
[62] A. Sultana, M. Sasaki, K. Suzuki, H. Hamada, *Catal. Commun.* **2013**, *41*, 21–25.
[63] P. N. Panahi, D. Salari, A. Niaei, S. M. Mousavi, *J. Ind. Eng. Chem.* **2013**, *19*, 1793–1799.
[64] T. Doan, A. Dang, D. Nguyen, T. Tran, T. H. Vuong, M. T. Le, T. H. Pham, *Viet. J. Chem.* **2021**, *59*, 935–942.
[65] E.-H. Yuan, M. Li, M.-H. Yang, X. Huang, K. Zhang, W. Han, Z. Tang, Z.-W. Liu, *Microporous Mesoporous Mater.* **2022**, *331*, 111675.
[66] T. Komatsu, H. Lin, T. Yashima, *Top. Catal.* **2000**, *10*, 73–77.
[67] P. S. Metkar, M. P. Harold, V. Balakotaiah, *Appl. Catal. B* **2012**, *111*, 67–80.
[68] P. S. Metkar, M. P. Harold, V. Balakotaiah, *Chem. Eng. Sci.* **2013**, *87*, 51–66.
[69] F. Bin, C. Song, G. Lv, J. Song, S. Wu, X. Li, *Appl. Catal. B* **2014**, *150–151*, 532–543.

[70] Y. Zhang, P. Wang, D. Yu, H. Zhao, X. Lyu, L. Lei, *J. Cen. South Uni.* **2022**, *29*, 2239–2252.
[71] X. Lou, P. Liu, J. Li, Z. Li, K. He, *Appl. Surf. Sci.* **2014**, *307*, 382–387.
[72] S. Zhang, C. Zhang, Q. Wang, W.-S. Ahn, *Ind. Eng. Chem. Res.* **2019**, *58*, 22857–22865.
[73] H. Xue, X. Guo, T. Meng, Q. Guo, D. Mao, S. Wang, *ACS Catal.* **2021**, *11*, 7702–7718.
[74] M. Salazar, R. Becker, W. Grünert, *Appl. Catal. B* **2015**, *165*, 316–327.
[75] M. Salazar, S. Hoffmann, O. P. Tkachenko, R. Becker, W. Grünert, *Appl. Catal. B* **2016**, *182*, 213–219.
[76] M. Salazar, S. Hoffmann, L. Tillmann, V. Singer, R. Becker, W. Grünert, *Appl. Catal. B* **2017**, *218*, 793–802.
[77] M. Salazar, S. Hoffmann, V. Singer, R. Becker, W. Grünert, *Appl. Catal. B* **2016**, *199*, 433–438.
[78] L. Zhang, D. Wang, Y. Liu, K. Kamasamudram, J. Li, W. Epling, *Appl. Catal. B* **2014**, *156*, 371–377.
[79] M. L. M. de Oliveira, C. M. Silva, R. Moreno-Tost, T. L. Farias, A. Jimenez-Lopez, E. Rodr'iguez-Castellón, *Appl. Catal. B* **2009**, *88*, 420–429.
[80] W. Liu, Y. Long, J. Zhang, S. Liu, Y. Zhou, X. Tong, Y. Yin, X. Li, K. Hu, J. Hu, *J. Environ. Chem. Eng.* **2022**, *10*, 108461.
[81] M. Shelef, *Chem. Rev.* **1995**, *95*, 209–225.
[82] X. Feng, W. K. Hall, *J. Catal.* **1997**, *166*, 368–376.
[83] R. G. Silver, M. O. Stefanick, B. I. Todd, *Catal. Today* **2008**, *136*, 28–33.
[84] L. Pang, C. Fan, L. Shao, K. Song, J. Yi, X. Cai, J. Wang, M. Kang, T. Li, *Chem. Eng. J.* **2014**, *253*, 394–401.
[85] C.-K. Seo, B. Choi, H. Kim, C.-H. Lee, C.-B. Lee, *Chem. Eng. J.* **2012**, *191*, 331–340.
[86] J. Guan, L. Zhou, W. Li, D. Hu, J. Wen, B. Huang, *Catalysts* **2021**, *11*, 324.
[87] H. Liu, Z. Chen, H. Wang, C. You, *Appl. Surf. Sci.* **2021**, *570*, 151105.
[88] S. Feng, W. Kong, Y. Wang, Y. Xing, Z. Wang, J. Ma, B. Shen, L. Chen, J. Yang, Z. Li, Ch. Zhang, *Fuel* **2023**, *353*, 129139.
[89] S. Feng, Z. Li, B. Shen, P. Yuan, B. Wang, L. Liu, Z. Wang, J. Ma, W. Kong, *Fuel* **2022**, *323*, 124337.
[90] J. Yang, Z. Li, C. Yang, Y. Ma, Y. Li, Q. Zhang, K. Song, J. Cui, *J. Solid State Chem.* **2022**, *305*, 122700.
[91] L. Chen, X. Wang, Q. Cong, H. Ma, S. Li, W. Li, *Chem. Eng. J.* **2019**, *369*, 957–967.
[92] X. Shi, F. Liu, L. Xie, W. Shan, H. He, *Environ. Sci. Technol.* **2013**, *47*, 3293–3298.
[93] S. H. I. Xiaoyan, L. I. U. Fudong, S. Wenpo, H. E. Hong, *Chin. J. Catal.* **2012**, *33*, 454–464.
[94] J. H. Kwak, D. Tran, S. D. Burton, J. Szanyi, J. H. Lee, C. H. F. Peden, *J. Catal.* **2012**, *287*, 203–209.
[95] X. Ye, R. Oord, M. Monai, J. E. Schmidt, T. Chen, F. Meirer, B. M. Weckhuysen, *Catal. Sci. Technol.* **2022**, *12*, 2589–2603.
[96] J. Ji, Y. Tang, L. Han, P. Ran, W. Song, Y. Cai, W. Tan, J. Sun, C. Tang, L. Dong, *Chem. Eng. J.* **2022**, *445*, 136530.
[97] J. H. Baik, S. D. Yim, I.-S. Nam, Y. S. Mok, J.-H. Lee, B. K. Cho, S. H. Oh, *Top. Catal.* **2004**, *30*, 37–41.
[98] T. Zhang, J. Shi, J. Liu, D. Wang, Z. Zhao, K. Cheng, J. Li, *Appl. Surf. Sci.* **2016**, *375*, 186–195.
[99] L. Zhang, T. Du, H. Qu, B. Chi, Q. Zhong, *Chem. Eng. J.* **2017**, *313*, 702–710.
[100] Y. Wang, X. Ji, H. Meng, L. Qu, X. Wu, *Catal. Commun.* **2020**, *138*, 105969.
[101] H. Jouini, I. Mejri, B. Rhimi, M. Mhamdi, T. Blasco, G. Delahay, *Res. Chem. Intermed.* **2021**, *47*, 2901–2915.
[102] H. Jouini, A. de Marcos-Galán, I. Mejri, R. Bensouilah, M. Mhamdi, T. Blasco, G. Delahay, *Inorganics* **2022**, *10*, 180.
[103] T. Du, H. Qu, Q. Liu, Q. Zhong, W. Ma, *Chem. Eng. J.* **2015**, *262*, 1199–1207.
[104] Z. Di, H. Wang, R. Zhang, H. Chen, Y. Wei, J. Jia, *Appl. Catal. A* **2022**, *630*, 118438.
[105] H. Jouini, I. Mejri, J. Martinez-Ortigosa, J. L. Cerillo, C. Petitto, M. Mhamdi, T. Blasco, G. Delahay, *Res. Chem. Intermed.* **2022**, *48*, 3415–3428.
[106] F. Gao, E. D. Walter, E. M. Karp, J. Luo, R. G. Tonkyn, J. H. Kwak, J. Szanyi, C. H. F. Peden, *J. Catal.* **2013**, *300*, 20–29.
[107] Y. Nakasaka, T. Kanda, K. Shimizu, K. Kon, G. Shibata, T. Masuda, *Catal. Today* **2019**, *332*, 64–68.
[108] H. Wang, J. Jia, S. Liu, H. Chen, Y. Wei, Z. Wang, L. Zheng, Z. Wang, R. Zhang, *Environ. Sci. Technol.* **2021**, *55*, 5422–5434.
[109] R. Srivastava, *Catal. Today* **2018**, *309*, 172–188.
[110] D. Verboekend, J. Pérez-Ramírez, *Chem. Eur. J.* **2011**, *17*, 1137–1147.
[111] Z.-F. Yan, Z. Li, K. He, J.-S. Zhao, X.-R. Lou, Z. Li, J.-S. Zhang, W. Huang, *Energy Sources Part A* **2016**, *38*, 315–321.
[112] M. Hartmann, M. Thommes, W. Schwieger, *Adv. Mater. Inter.* **2021**, *8*, 2001841.
[113] M. Hartmann, A. G. Machoke, W. Schwieger, *Chem. Soc. Rev.* **2016**, *45*, 3313–3330.
[114] D. Verboekend, R. Caicedo-Realpe, A. Bonilla, M. Santiago, J. Perez-Ramírez, *Chem. Mater.* **2010**, *22*, 4679–4689.
[115] W. Schwieger, A. G. Machoke, T. Weissenberger, A. Inayat, T. Selvam, M. Klumpp, A. Inayat, *Chem. Soc. Rev.* **2016**, *45*, 3353–3376.
[116] X. Jia, W. Khan, Z. Wu, J. Choi, A. C. K. Yip, *Adv. Powder Technol.* **2019**, *30*, 467–484.
[117] S. Lopez-Orozco, A. Inayat, A. Schwab, T. Selvam, W. Schwieger, *Adv. Mater.* **2011**, *23*, 2602–2615.
[118] D. Verboekend, S. Mitchell, M. Milina, J. C. Groen, J. Pérez-Ramírez, *J. Phys. Chem. C* **2011**, *115*, 14193–14203.
[119] D. Verboekend, J. Pérez-Ramírez, *ChemSusChem* **2014**, *7*, 753–764.
[120] J. Liu, F. Yu, J. Liu, L. Cui, Z. Zhao, Y. Wei, Q. Sun, *J. Environ. Sci.* **2016**, *48*, 45–58.
[121] Z. Xie, X. Zhou, H. Wu, L. Chen, H. Zhao, Y. Liu, L. Pan, H. Chen, *Sci. Rep.* **2016**, *6*, 1–9.
[122] D. Verboekend, N. Nuttens, R. Locus, J. Van Aelst, P. Verolme, J. C. Groen, J. Pérez-Ramírez, B. F. Sels, *Chem. Soc. Rev.* **2016**, *45*, 3331–3352.
[123] J. Pérez-Ramírez, C. H. Christensen, K. Egeblad, C. H. Christensen, J. C. Groen, *Chem. Soc. Rev.* **2008**, *37*, 2530–2542.
[124] D. Verboekend, G. Vilé, J. Pérez-Ramírez, *Adv. Funct. Mater.* **2012**, *22*, 916–928.
[125] L. Chmielarz, R. Dziembaj, *Catalysts* **2021**, *11*, 644.
[126] M. Jabłońska, K. Góra-Marek, M. Grilc, P. C. Bruzzese, D. Poppitz, K. Pyra, M. Liebau, A. Pöppl, B. Likozar, R. Gläser, *Catalysts* **2021**, *11*, 843.
[127] M. Rutkowska, I. Pacia, S. Basąg, A. Kowalczyk, Z. Piwowarska, M. Duda K. A. Tarach, K. Góra-Marek, M. Michalik, U. Díaz, L. Chmielarz, *Microporous Mesoporous Mater.* **2017**, *246*, 193–206.
[128] J. C. Groen, J. C. Jansen, J. A. Moulijn, J. Pérez-Ramírez, *J. Phys. Chem. B* **2004**, *108*, 13062–13065.
[129] J. C. Groen, L. A. A. Peffer, J. A. Moulijn, J. Pérez-Ramírez, *Colloids Surf. A* **2004**, *241*, 53–58.
[130] K. Góra-Marek, K. Brylewska, K. A. Tarach, M. Rutkowska, M. Jabłońska, M. Choi, L. Chmielarz, *Appl. Catal. B* **2015**, *179*, 589–598.
[131] A. L. Kustov, K. Egeblad, M. Kustova, T. W. Hansen, C. H. Christensen, *Top. Catal.* **2007**, *45*, 159–163.
[132] M. Rutkowska, A. Borcuch, A. Marzec, A. Kowalczyk, B. Samojeden, J. M. Moreno, U. Díaz, L. Chmielarz, *Microporous Mesoporous Mater.* **2020**, *304*, 109114.
[133] J. Ma, D. Weng, X. Wu, Z. Si, Z. Wu, *Prog. Nat. Sci. Mater. Int.* **2013**, *23*, 493–500.
[134] T. Johannessen, H. Schmidt, A. M. Frey, C. H. Christensen, *Catal. Lett.* **2009**, *128*, 94–100.
[135] J. C. Groen, J. Pérez-Ramírez, L. A. A. Peffer, *Chem. Lett.* **2002**, *31*, 94–95.
[136] J. C. Groen, L. A. A. Peffer, J. Pérez-Ramírez, *Microporous Mesoporous Mater.* **2003**, *60*, 1–17.
[137] J. C. Groen, J. Pérez-Ramírez, *Appl. Catal. A* **2004**, *268*, 121–125.
[138] Y. Yue, H. Liu, P. Yuan, C. Yu, X. Bao, *Sci. Rep.* **2015**, *5*, 1–10.
[139] Y. Yue, B. Liu, N. Lv, T. Wang, X. Bi, H. Zhu, P. Yuan, Z. Bai, Q. Cui, X. Bao, *ChemCatChem* **2019**, *11*, 4744–4754.
[140] Y. Ma, Y. Liu, Z. Li, C. Geng, X. Bai, D. Cao, *Environ. Sci. Pollut. Res. Int.* **2020**, *27*, 9935–9942.
[141] C. Peng, R. Yan, H. Peng, Y. Mi, J. Liang, W. Liu, X. Wang, G. Song, P. Wu, F. Liu, *J. Hazard. Mater.* **2020**, *385*, 121593.
[142] R. Yan, S. Lin, Y. Li, W. Liu, Y. Mi, C. Tang, L. Wang, P. Wu, H. Peng, *J. Hazard. Mater.* **2020**, *396*, 122592.
[143] B. Liu, K. Zheng, Z. Liao, P. Chen, D. Chen, Y. Wu, Q. Xia, H. Xi, J. Dong, *Ind. Eng. Chem. Res.* **2020**, *59*, 8592–8600.
[144] L. Wang, Y. Ren, X. Yu, C. Peng, D. Yu, C. Zhong, J. Hou, C. Yin, X. Fan, Z. Zhao, J. Liu, Y. Wei, *J. Catal.* **2023**, *417*, 226–247.
[145] P. S. Metkar, V. Balakotaiah, M. P. Harold, *Chem. Eng. Sci.* **2011**, *66*, 5192–5203.
[146] C. Zhong, J. Gong, L. Tan, W. Liu, G. Liu, Z. Zhang, *Chem. Eng. Sci.* **2019**, *207*, 479–489.
[147] S. Yu, J. Zhang, *Processes* **2021**, *9*, 1966.
[148] H. Jeong, H.-J. Ha, G. Kim, C.-W. Ahn, B.-D. Hahn, W.-H. Yoon, J.-J. Choi, J.-H. Choi, *Catal. Today* **2023**, *425*, 114317.
[149] R. Raju, N. Gomathi, K. Prabhakaran, K. Joseph, A. Salih, *React. Chem. Eng.* **2022**, *7*, 929–942.

[150] J. Ochońska-Kryca, M. Iwaniszyn, M. Piątek, P. J. Jodłowski, J. Thomas, A. Kołodziej, J. Łojewska, *Catal. Today* **2013**, *216*, 135–141.
[151] J. Kryca, P. J. Jodłowski, M. Iwaniszyn, B. Gil, M. Sitarz, A. Kołodziej, T. Łojewska, J. Łojewska, *Catal. Today* **2016**, *268*, 142–149.
[152] J. Ochońska, D. McClymont, P. J. Jodłowski, A. Knapik, B. Gil, W. Makowski, W. Łasocha, A. Kołodziej, S. T. Kolaczkowski, J. Łojewska, *Catal. Today* **2012**, *191*, 6–11.
[153] P. J. Jodłowski, Ł. Kuterasiński, R. J. Jędrzejczyk, D. Chlebda, A. Gancarczyk, S. Basąg, L. Chmielarz, *Catalysts* **2017**, *7*, 205.
[154] Q. Yuan, Z. Zhang, N. Yu, B. Dong, *Catal. Commun.* **2018**, *108*, 23–26.
[155] E. M. Cepollaro, R. Botti, G. Franchin, L. Lisi, P. Colombo, S. Cimino, *Catalysts* **2021**, *11*, 1212.
[156] M. Jabłońska, *RSC Adv.* **2022**, *12*, 25240–25261.
[157] M. Jabłońska, *J. Mol. Catal.* **2022**, *518*, 112111.
[158] A. Grossale, I. Nova, E. Tronconi, D. Chatterjee, M. Weibel, *J. Catal.* **2008**, *256*, 312–322.
[159] M. P. Ruggeri, A. Grossale, I. Nova, E. Tronconi, H. Jirglova, Z. Sobalik, *Catal. Today* **2012**, *184*, 107–114.
[160] L. Chen, S. Ren, L. Liu, B. Su, J. Yang, Z. Chen, M. Wang, Q. Liu, *J. Environ. Chem. Eng.* **2022**, *10*, 107167.
[161] H. Xue, X. Guo, T. Meng, D. Mao, Z. Ma, *Surf. Interfaces* **2022**, *29*, 101722.
[162] S. A. Yashnik, Z. R. Ismagilov, *Appl. Catal. A* **2021**, *615*, 118054.
[163] K. A. Tarach, M. Jabłońska, K. Pyra, M. Liebau, B. Reiprich, R. Gläser, K. Góra-Marek, *Appl. Catal. B* **2021**, *284*, 119752.
[164] M. P. Ruggeri, T. Selleri, M. Colombo, I. Nova, E. Tronconi, *J. Catal.* **2014**, *311*, 266–270.
[165] R. P. Vélez, I. Ellmers, H. Huang, U. Bentrup, V. Schünemann, W. Grünert, A. Brückner, *J. Catal.* **2014**, *316*, 103–111.
[166] R. P. Vélez, U. Bentrup, W. Grünert, A. Brückner, *Top. Catal.* **2017**, *60*, 1641–1652.
[167] M. Agote-Arán, I. Lezcano-González, A. G. Greenaway, S. Hayama, S. Díaz-Moreno, A. B. Kroner, A. M. Beale, *Appl. Catal. A* **2019**, *570*, 283–291.
[168] A. Boubnov, H. W. P. Carvalho, D. E. Doronkin, T. Günter, E. Gallo, A. J. Atkins, C. R. Jacob, J.-D. Grunwaldt, *J. Am. Chem. Soc.* **2014**, *136*, 13006–13015.
[169] L. J. Lobree, I.-C. Hwang, J. A. Reimer, A. T. Bell, *J. Catal.* **1999**, *186*, 242–253.
[170] D. Wierzbicki, A. H. Clark, O. Kröcher, D. Ferri, M. Nachtegaal, *J. Phys. Chem. C* **2022**, *126*, 17510–17519.
[171] B. F. Mentzen, G. Bergeret, *J. Phys. Chem. C* **2007**, *111*, 12512–12516.
[172] D. E. Doronkin, M. Casapu, T. Günter, O. Müller, R. Frahm, J.-D. Grunwaldt, *J. Phys. Chem. C* **2014**, *118*, 10204–10212.
[173] N.-Y. Topsøe, M. Anstrom, J. A. Dumesic, *Catal. Lett.* **2001**, *76*, 11–20.
[174] M. Schwidder, M. S. Kumar, U. Bentrup, J. Pérez-Ramírez, A. Brückner, W. Grünert, *Microporous Mesoporous Mater.* **2008**, *111*, 124–133.
[175] M. P. Ruggeri, T. Selleri, I. Nova, E. Tronconi, J. A. Pihl, T. J. Toops, W. P. Partridge, *Top. Catal.* **2016**, *59*, 907–912.
[176] X. Shi, Y. Wang, Y. Shan, Y. Yu, H. He, *J. Environ. Sci.* **2020**, *94*, 32–39.
[177] P. Chen, M. Jabłońska, P. Weide, T. Caumanns, T. Weirich, M. Muhler, R. Moos, R. Palkovits, U. Simon, *ACS Catal.* **2016**, *6*, 7696–7700.
[178] V. F. Kispersky, A. J. Kropf, F. H. Ribeiro, J. T. Miller, *Phys. Chem. Chem. Phys.* **2012**, *14*, 2229–2238.
[179] A. M. Beale, F. Gao, I. Lezcano-Gonzalez, C. H. F. Peden, J. Szanyi, *Chem. Soc. Rev.* **2015**, *44*, 7371–7405.
[180] C. Paolucci, J. R. Di Iorio, W. F. Schneider, R. Gounder, *Acc. Chem. Res.* **2020**, *53*, 1881–1892.
[181] C. Paolucci, I. Khurana, A. A. Parekh, S. Li, A. J. Shih, H. Li, J. R. Di Iorio, J. D. Albarracin-Caballero, A. Yezerets, J. T. Miller, W. N. Delgass, F. H. Ribeiro, W. F. Schneider, R. Gounder, *Science* **2017**, *357*, 898–903.
[182] S. T. Korhonen, D. W. Fickel, R. F. Lobo, B. M. Weckhuysen, A. M. Beale, *Chem. Commun.* **2011**, *47*, 800–802.
[183] M. Moreno-González, B. Hueso, M. Boronat, T. Blasco, A. Corma, *J. Phys. Chem. Lett.* **2015**, *6*, 1011–1017.
[184] I. Lezcano-González, D. S. Wragg, W. A. Slawinski, K. Hemelsoet, A. Van Yperen-De Deyne, M. Waroquier, V. Van Speybroeck, A. M. Beale, *J. Phys. Chem. C* **2015**, *119*, 24393–24403.
[185] P. Chen, A. Khetan, M. Jabłońska, J. Simböck, M. Muhler, R. Palkovits, H. Pitsch, U. Simon, *Appl. Catal. B* **2018**, *237*, 263–272.
[186] J. Abdul Nasir, J. Guan, T. W. Keal, A. W. Desmoutier, Y. Lu, A. M. Beale, C. R. A. Catlow, A. A. Sokol, *J. Am. Chem. Soc.* **2022**, *145*, 247–259.
[187] A. G. Greenaway, A. Marberger, A. Thetford, I. Lezcano-González, M. Agote-Arán, M. Nachtegaal, D. Ferri, O. Kröcher, C. R. A. Catlow, A. M. Beale, *Chem. Sci.* **2020**, *11*, 447–455.

Manuscript received: September 28, 2023
Revised manuscript received: November 30, 2023
Accepted manuscript online: December 6, 2023
Version of record online: January 26, 2024

REVIEW

Transition metal-containing MFI-based catalysts are widely investigated in NH_3-SCR-DeNO$_x$ and NH_3-SCO. Our review gives a critical overview of the influence of introducing mesopores on the catalyst activity and N_2 selectivity as well as the strategies for the development of ZSM-5 based catalysts with enhanced catalytic lifetime, supported by the investigations of reaction mechanisms.

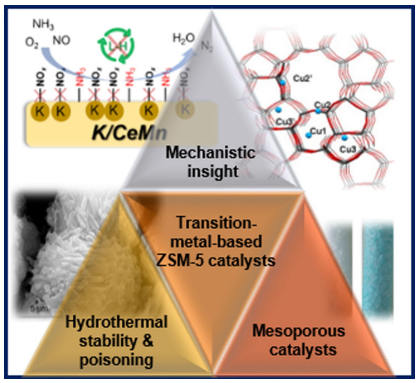

Dr. Eng. M. Jabłońska, Dr. M. E. Potter, Prof. Dr. A. M. Beale**

1 – 21

Recent Progress in the Application of Transition-Metal Containing MFI topologies for NH_3-SCR-DeNO$_x$ and NH_3 oxidation